Jointly Optimized Beamforming and Power Allocation for Full-Duplex Cell-Free NOMA in Space-Ground Integrated Networks

Qiling Gao, Min Jia, *Senior Member, IEEE*, Qing Guo, *Member, IEEE*, Xuemai Gu, *Member, IEEE* and Lajos Hanzo, *Life Fellow, IEEE*

***Abstract*—Space-ground integrated networks (SGINs) have attracted substantial research interests due to their wide area coverage capability, where spectrum sharing is employed between the satellite and terrestrial networks for improving the spectral efficiency (SE). We further improve the SE by conceiving a cell-free system in SGINs, where the full-duplex (FD) multi-antenna APs simultaneously provide downlink and uplink services at the same time and within the same frequency band. Furthermore, power domain (PD) non-orthogonal multiple access (NOMA) is employed as the multiple access (MA) technique in the cell-free system. To achieve a performance enhancement, the sum-rate maximization problem is formulated for jointly optimizing the power allocation factors (PAFs) of the NOMA downlink (DL), the uplink transmit power, and both the beamformer of the satellite and of the APs. Successive convex approximation (SCA) and semi-definite programming (SDP) are adopted to transform the resultant non-convex problem into an equivalent convex one. Our simulation results reveal that 1) our proposed system outperforms the well-known approaches (i.e., frequency division duplex (FDD) and small cell systems) in terms of its SE; 2) our proposed optimization algorithm significantly improves the networking performance; 3) the conceived SIC order design outperforms the fixed-order design at the same complexity.**

***Index Terms*—Beamforming design, cell-free, full-duplex, multiple-antenna NOMA, power allocation, SAGINs.**

I. Introduction

FUTURE networks are expected to cope with the explosive proliferation of wireless devices requiring seamless coverage [1]. However, purely depending on terrestrial networks cannot provide ubiquitous services at any place on the earth [2], [3]. Hence, the framework of space-ground integrated networks (SGINs) is becoming ubiquitous in support of the global multimedia communications infrastructure [4], [5]. In contrast to hybrid satellite-terrestrial networks (HSTNs), where the terrestrial components operate independently from the satellites, the proposed evolved SGINs offer an opportunity for spectrum sharing between the satellite and terrestrial networks to alleviate the spectrum scarcity problem [6]. However, given the requirements of broadband services and the limited availability of L and S-band spectral resources, frequency bands above 10 GHz (i.e., Ku and Ka bands) have been assigned for satellite services [7]. Moreover, thanks to the maturing development of mmWave techniques for the terrestrial layer, the lower mmWave bands may find application in 6G [8]. Hence, it is of paramount importance to study spectrum sharing in the context of Ka-band between the satellite and terrestrial networks to mitigate the spectrum scarcity of the sub-6 GHz bands. The integration of networks increases their flexibility, exacerbates their joint resource management [9]. Sophisticated techniques have been proposed for the joint resource allocation in SGINs [10], [11].

Recently, cell-free systems have been widely recognized as a practically viable technique of mitigating the cell-edge problem as well as improving the energy efficiency, coverage, and spectral efficiency (SE) [12]. In the cell-free system, multiple access points (APs) having a small number of antennas are geographically spread out and connected via the fronthaul link to the central processing unit (CPU) for coordination and data processing [13]. Since multiple APs can serve a group of users without observing any cell boundaries, the cell-free system is capable of providing macro-diversity gains by mitigating fading, thereby enhancing the system performance [14]–[16]. On the other hand, power-domain (PD) non-orthogonal multiple access (NOMA) has been widely advocated for improving the number of users supported by allowing more than one user to share a specific resource slot [17]. The combination of NOMA with the cell-free technique has the potential of reaping joint benefits in support of massive connectivity [18], [19]. In contrast to the conventional small-cell NOMA where the users are served by co-located antennas at an AP, in cell-free systems, users are served by a group of distributed antennas, which results in additional degrees-of-freedom for improving networking performance.

A. Motivation and Contributions

Given the thirst for bandwidth, the terrestrial and satellite networks may potentially benefit from spectrum sharing [20]. As a further promising technique, full-duplex (FD) cell-free

Q. Gao is with the School of Electronics and Information Engineering, Harbin Institute of Technology, Harbin, 150008, China, and also with the School of Electronics and Computer Science, University of Southampton, Southampton, SO17 1BJ, U.K. (email: 18B905013@stu.hit.edu.cn).

M. Jia, Q. Guo and X. Gu are with the School of Electronics and Information Engineering, Harbin Institute of Technology, Harbin, 150008, China (email: jiamin@hit.edu.cn, qguo@hit.edu.cn, guxuemai@hit.edu.cn). Corresponding author: Min Jia.

L. Hanzo is with the School of Electronics and Computer Science, University of Southampton, Southampton, SO17 1BJ, U.K. (e-mail: lh@ecs.soton.ac.uk).

The work of M. Jia was supported by National Natural Science Foundation of China No. 62231012, National Key Research and Development Program of China under Grant 2021YFB2900500, and Natural Science Foundation for Outstanding Young Scholars of Heilongjiang Province under Grant YQ2020F001.

L. Hanzo would like to acknowledge the financial support of the Engineering and Physical Sciences Research Council projects EP/W016605/1 and EP/X01228X/1 as well as of the European Research Council's Advanced Fellow Grant QuantCom (Grant No. 789028).

Table I: BOLDLY AND EXPLICITLY CONTRASTING OUR CONTRIBUTIONS TO THE LITERATURE

	Our Paper	[21]-2020	[22]-2020	[23]-2020	[24]-2019	[25]-2019	[26]-2019	[27]-2017
Cell-free NOMA in SGINs	✓							
Joint UL and DL design	✓							
Cell-free architecture	✓	✓	✓	✓	✓		✓	✓
Power domain NOMA	✓	✓	✓	✓		✓		
Full-duplex scheme	✓				✓			
Multi-antenna APs	✓	✓	✓	✓	✓			

NOMA offers tremendous potential in terms of improving the SE for the following reasons: 1) the cell-free system concept has the benefit of assigning the AP antennas close to the users, hence reducing the propagation loss between them as well as achieving improved load balancing; 2) the cell-free system provides additional design flexibility for NOMA, since each AP is capable of independent power allocation and beamforming design; 3) the employment of FD and NOMA facilitates spectrum sharing between the uplink (UL) and downlink (DL) as well as among users, therefore may increase the SE.

Inspired by the aforementioned advantages, in this paper, we propose for the first time the NOMA-aided FD cell-free SGINs concept for the improving the SE. However, the interference among different networks due to the satellite-terrestrial spectrum sharing as well as interference introduced by the application of FD and NOMA (e.g., the residual self-interference (SI), the co-channel interference (CCI), and the inter-user interference (IUI)) results in non-negligible networking performance degradation, and imposes challenges on the resource management. Therefore, we conceive joint satellite and terrestrial beamforming as well as power allocation for mitigating the interference, hence enhance the sum-rate, while taking into account the effects of realistic imperfect channel estimation and the imperfect successive interference cancellation (SIC). The main contributions of this paper are boldly and explicitly contrasted to the state-of-the-art at a glance in Table I. To elaborate:

- We propose FD cell-free NOMA aided SGINs, where the satellite users (SUs) are served by the satellite directly within the same frequency band as the terrestrial networks (Ka band). In the terrestrial layer, the FD-enabled multiple-antenna APs support both the uplink users (UUs) and the downlink users (DUs) within the same time/frequency resource by relying on the cell-free construction. Again, PD NOMA is employed as the multiple access (MA) technique in the cell-free system.
- We formulate a sum-rate maximization problem for the joint optimization of the NOMA DL power allocation factors, of the UL transmit power and of the beamformer of both the APs as well as of the satellite. The resultant non-convex problem is solved by employing successive convex approximation (SCA) and semi-definite programming (SDP) methods. Additionally, we propose an efficient SIC order configuration for the NOMA DL.
- We demonstrate the superiority of our proposed system as well as of the optimization algorithm. Our numerical results confirm that 1) the proposed system outperforms the frequency division duplex (FDD) based cell-free NOMA/OMA and FD cell-based NOMA systems in terms of SE; 2) the sum-rate performance can be significantly enhanced by employing our proposed optimization algorithm; 3) the distributed multiple APs improve the system's design flexibility.

B. Organization and Notation

The rest of this paper is organized as follows. Section II discusses the related prior art. The system model is introduced in Section III. Then the optimization problem is formulated in Section IV and the proposed optimization algorithm is detailed in Section V. In Section VI, our simulation results are discussed, demonstrating the performance enhancements attained, followed by our conclusion in Section VII.

Notation: $(\cdot)^{\dagger}$, $\mathrm{Tr}(\cdot)$ and $\mathrm{Rank}(\cdot)$ stand for the Hermitian transpose, trace and rank of a matrix, $\|\cdot\|$ and $|\cdot|$ denote the Euclidean norm and absolute value, $\mathbb{C}^{M\times N}$ defines the complex space of $M \times N$, $\mathbf{A} \succeq \mathbf{0}$ means that matrix $\mathbf{A}$ is a positive semi-definite matrix.

II. STATE-OF-THE-ART

The advantages of the SGINs concept have inspired both industry and academia [28]–[30]. In this context, spectrum sharing is a natural solution for the efficient exploitation of the limited spectral resources as demonstrated in [31], [32]. In [31], both the uplink and downlink interference was analyzed. In [32], Liang *et al.* conceived an artificial intelligence based spectrum sharing scheme for SGINs. In addition to spectrum sharing, NOMA and other sophisticated techniques have been proposed for SGINs for the improved SE [25].

A. Studies on NOMA aided SGINs

NOMA has been widely recognized as a promising technique of enhancing the SE by increasing the number of users [17], therefore its application in SGINs has received substantial research attention [20]. In [19], Zhu *et al.* investigated a general non-orthogonal SGINs downlink transmission framework, in which both the beamforming and power allocation was optimized for maximizing the system capacity. In [25], Lin *et. al* studied the sum-rate maximization problem of NOMA assisted SGINs by jointly designing the beamforming and power allocation, where the satellite shares the spectrum with terrestrial NOMA assisted cellular networks. In [33], the energy efficiency and system capacity of NOMA-based SGINs were maximized by jointly designing the user

clustering, beamforming and power allocation. In [34], Li *et al.* studied the sum secrecy rate maximization by designing the beamforming of NOMA-based SGINs, where NOMA was only employed in the terrestrial layer. Tang *et al.* [35] derived the outage probability expressions of NOMA-based SGINs by taking into account the impact of hardware impairments. Furthermore, the authors of [36] derived the outage probability of multiple-antenna relay-aided NOMA-based SGINs.

B. Studies on cell-free systems

Again, the cell-free system concept is promising, since it offers improved spectral- and energy efficiency, albeit at the cost of increasing the backhaul requirements [13]. The closed-form downlink SE expression of cell-free systems was derived in [26], while accounting for effects of channel estimation errors. The authors of [37] studied the utility maximization problem by designing the power control of APs in the downlink of cell-free systems, where the SE, proportional fairness, and harmonic rate were used as system-wide utility functions. The authors of [38] proposed a non-orthogonal backhaul design for cell-free massive MIMO systems, while the authors of [39] studied the average downlink rate of cell-free systems with an emphasis on pilot assignment algorithms. In [40], Wang *et al.* studied the rate maximization problem in the downlink of cell-free systems, where the bisection method was adopted for the power control design.

C. Studies on NOMA assisted cell-free systems

The potential performance gains of combining the cell-free and NOMA concepts have been widely investigated [12], [41]. The authors of [12] derived the asymptotic achievable rate of NOMA aided cell-free systems by employing the stochastic geometry approach, under the assumption of realistic imperfect successive cancellation (SIC). In [21], Rezaei *et al.* derived closed-form sum-rate expressions for characterizing the downlink of cell-free NOMA systems, where maximum ratio transmission (MRT), full-pilot based zero-forcing (fpZF), and modified regularized ZF (mRZF) were employed at the APs. The authors of [22] proposed a power control scheme for maximizing the minimal rate of users in the cell-free NOMA system. The authors of [23] investigated the user clustering issues of the cell-free NOMA downlink with the objective of maximizing the sum-rate, where the resultant non-convex problem was solved by learning-based algorithms. In [41], Li *et. al* compared the sum-rate of NOMA-aided cell-free systems to that of their OMA counterpart.

III. System Model

The SGINs considered are shown in Fig. 1, where N_s SUs are served by the satellite DL within the same frequency band as the terrestrial networks. The FD cell-free NOMA system is employed in the terrestrial layer, where M APs are equipped with FD capability by relying on circulator-based FD radio prototypes, and connected to the CPU via perfect optical back-haul links [24]. All these APs simultaneously serve KN downlink users (DUs) and N_u uplink users (UUs) in the same time and frequency resources. Each AP is equipped with L_m antennas, and the total number of antennas of all APs is $L = \sum_{m=1}^{M} L_m$, while each user has a single antenna. Specifically, for the uplink, the UUs simultaneously broadcast

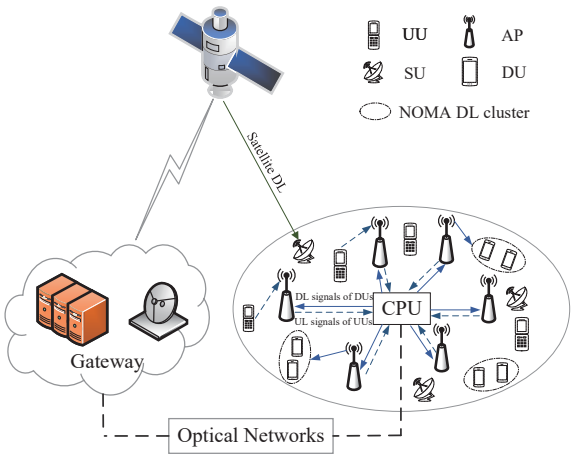

Figure 1: Illustration of the cell-free NOMA aided SGINs.

their signals to all APs and the received signal of all APs can be aggregated and processed at the CPU. The DUs are assigned into N clusters with K users per cluster and served by all APs via the NOMA DL. Our proposed system offers the following advantages 1) improving the sum-rate for a given system bandwidth; 2) providing additional degrees-of-freedom for the network design.

Despite the aforementioned potential, both the spectrum sharing between satellite and terrestrial networks as well as the FD scheme employed at APs, and the NOMA scheme inflict additional interference (e.g., SI, CCI, and IUI), which degrades the SE and imposes challenges on the optimization. To be specific, both the desired signal and the interference links of Fig. 1 are explicitly defined in Fig. 2 and the symbol descriptions are shown in Table II.

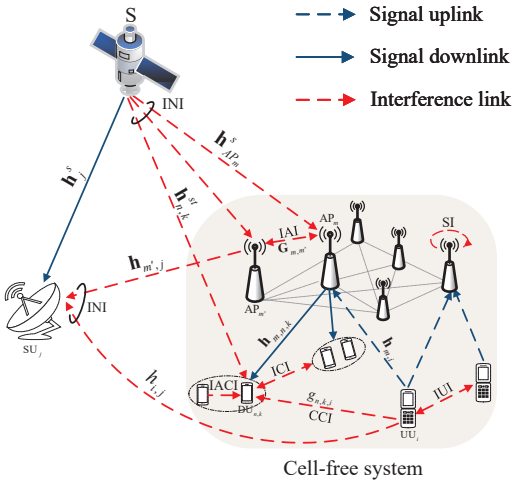

Figure 2: Signal and interference illustration of the FD cell-free NOMA aided SGINs.

- In the cell-free UL, the UUs simultaneously transmit their UL signals to all the APs, which causes IUI. The APs can receive both the other APs' DL signals as well as their own DL signals, referred to as the inter-AP interference (IAI) and the SI, respectively. Moreover, the APs can also receive the satellite's DL signals, termed as the inter-net interference (INI).

- In the cell-free DL, the DUs are served by all the APs via the NOMA DL. Hence a DU's received signals include the signals of other DUs in the same cluster, termed as the intra-cluster (IACI) interference, and the signals of other clusters, defined as the inter-cluster interference (ICI), the UL signals of the UUs, referred to as the CCI and the satellite's DL signals, defined as the INI.
- In the satellite DL, the SUs receive the satellite DL broadcasting signals as well as the UL signals of the UUs and the DL signals transmitted by the APs,

Table II: DESCRIPTION OF THE SYMBOLS

Symbol	Definition
$\mathbf{h}_{m,n,k}$	Channel between the $\text{DU}_{n,k}$ and the AP_m
$\mathbf{h}^{st}_{n,k}$	Channel vector between the $\text{DU}_{n,k}$ and the satellite
$\mathbf{h}^{s}_{AP_m}$	Channel vector between the AP_m and the satellite
$\mathbf{h}_{m,j}$	Channel vector between the AP_m and the SU_j
$\mathbf{h}_{m,i}$	Channel vector between the UU_i and the AP_m
$\mathbf{G}_{m,m'}$	Channel vector between the AP_m and the $\text{AP}_{m'}$
$g_{n,k,i}$	Channel between the UU_i and the $\text{DU}_{n,k}$
$\mathbf{h}^{s}_{j}$	Channel vector between the SU_j and the satellite
$h_{i,j}$	Channel vector between the UU_i and the SU_j
$p_{n,k}$	Power allocation factors of the $\text{DU}_{n,k}$
$\mathbf{w}_{m,n}$	Beamforming vector of the n-th cluster at the m-th AP
$\mathbf{w}_s$	Beamforming vector at the satellite
p^u_i	Uplink transmit power of the UU_i
$\Gamma^d_{n,k\to k}$	Achievable rate of the $\text{DU}_{n,k}$
$\Gamma^d_{n,\tilde{k}\to k}$	Detecting rate of the $\text{DU}_{n,k}$ at the $\text{DU}_{n,\tilde{k}}$
Γ^u_i	Achievable rate of the UU_i
Γ_j	Achievable rate of the SU_j
$P^{\max}_{AP}$	Maximal transmit power of the AP
P_s	Maximal transmit power of the satellite
$P^{\max}_i$	Maximal transmit power of the UU_i
$\pi_n(k)$	SIC order of the $\text{DU}_{n,k}$
$\gamma^d_{n,k}$, γ^u_i, γ_j	Minimal required rate of $\text{DU}_{n,k}$, UU_i and SU_j
$\tilde{p}_p$	Pilot transmit power
σ^2, σ^2_s	Noise power

A. Signal Transmission

1) DL Transmission in Cell-free Systems: The DL signal of the n-th NOMA cluster can be expressed as $s_n = \sum_{k=1}^{K} \sqrt{p_{n,k}} s_{n,k}$, where $s_{n,k}$ is the DL signal of the $\text{DU}_{n,k}$, while $p_{n,k}$ is the power allocation factor of the $\text{DU}_{n,k}$, which is optimized in this paper. Then, the AP_m's transmitted DL signal can be expressed as

$$\mathbf{x}_m = \sum_{n=1}^{N} \mathbf{w}_{m,n} s_n, \tag{1}$$

where $\mathbf{w}_{m,n} \in \mathbb{C}^{L_m \times 1}$ represents the beamforming vector of the AP_m used for the n-th NOMA DL cluster. We first propose the SIC order for NOMA users as seen in *Remark* 1.

Remark 1. Based on the NOMA principle, SIC is employed to remove the intra-cluster interference. We define $\pi_n(k)$ as the SIC order of the $\text{DU}_{n,k}$, for any two users k and l, $\pi_n(k) > \pi_n(l)$ represents that the $\text{DU}_{n,k}$ detects the $\text{DU}_{n,l}$'s signal before detecting its own signal. Generally, the users with the poor effective channel gains are allocated with the higher power allocation factors and detected in priority. Moreover, the effective channel gains are relevant to our designed beamforming vectors $\mathbf{w}_{m,n}$ and $\mathbf{w}_s$. Hence, the SIC order of users may changed due to the changed value of $\mathbf{w}_{m,n}$ and $\mathbf{w}_s$ after each optimization, which may lead to high complexity as well as even to infeasibility. To develop a low-complexity SIC order decision regime without relying on the beamforming vectors, we propose a channel gain based SIC order, explicitly, if $\sum_{m=1}^{M} |\mathbf{h}_{m,n,l}|^2 > \sum_{m=1}^{M} |\mathbf{h}_{m,n,k}|^2$, then we have $\pi_n(l) > \pi_n(k)$.

Once the SIC order is defined, the DL signal received by the $\text{DU}_{n,k}$ after performing SIC can be expressed as

$$\begin{aligned} y_{n,k} = & \underbrace{\sum_{m=1}^{M} \mathbf{h}_{m,n,k} \mathbf{w}_{m,n} \sqrt{p_{n,k}} s_{n,k}}_{\text{desired signal}} \\ & + \underbrace{\sum_{m=1}^{M} \mathbf{h}_{m,n,k} \mathbf{w}_{m,n} \sum_{\pi_n(l) > \pi_n(k)} \sqrt{p_{n,l}} s_{n,l}}_{\text{intra-cluster interference}} \\ & + \underbrace{\sum_{i=1}^{N_u} \sqrt{p^u_i} g_{n,k,i} s^u_i}_{\text{CCI}} + \underbrace{\sum_{m=1}^{M} \mathbf{h}_{m,n,k} \sum_{n' \neq n} \mathbf{w}_{m,n'} s_{n'}}_{\text{ICI}} \\ & + \underbrace{\mathbf{h}^{st}_{n,k} \mathbf{w}_s s_{sat}}_{\text{INI}} + n_{n,k}, \end{aligned} \tag{2}$$

where $\mathbf{h}_{m,n,k}$ is the channel between the AP_m and the $\text{DU}_{n,k}$, p^u_i is the UL transmit power of the UU_i, $g_{n,k,i}$ is the channel between the UU_i and the $\text{DU}_{n,k}$, s^u_i is the UL signal of the UU_i, $s_{n'}$ is the signal of the n'-th cluster, $\mathbf{h}^{st}_{n,k} \in \mathbb{C}^{1 \times N_s}$ is the channel between the satellite and the $\text{DU}_{n,k}$, $\mathbf{w}_s \in \mathbb{C}^{N_s \times 1}$ is the beamforming vector of the satellite, s_{sat} is the satellite's DL signal, and finally $n_{n,k} \sim \mathcal{CN}\left(0, \sigma^2\right)$ represents the additive white Gaussian noise (AWGN) having a noise variance of σ^2.

The achievable rate for the $\text{DU}_{n,k}$ detecting its own signal is $R_{n,k\to k} = \log_2\left(1 + \Gamma^d_{n,k\to k}\right)$, $\Gamma^d_{n,k\to k}$ can be expressed as

$$\Gamma^d_{n,k\to k} = \frac{p_{n,k} \left| \sum_{m=1}^{M} \mathbf{h}_{m,n,k} \mathbf{w}_{m,n} \right|^2}{\chi_{n,k}}, \tag{3}$$

where $\chi_{n,k}$ is the interference at the $\text{DU}_{n,k}$, $\chi_{n,k} = \sum_{\pi_n(l) > \pi_n(k)} \left| \sum_{m=1}^{M} \mathbf{h}_{m,n,k} \mathbf{w}_{m,n} \sqrt{p_{n,l}} \right|^2 + \sum_{i=1}^{N_u} p^u_i |g_{n,k,i}|^2 + \sigma^2 + \sum_{n' \neq n}^{N} \left| \sum_{m=1}^{M} \mathbf{h}_{m,n,k} \mathbf{w}_{m,n'} \right|^2 + \left| \mathbf{h}^{st}_{n,k} \mathbf{w}_s \right|^2$.

Furthermore, for any $\text{DU}_{n,\tilde{k}}$ satisfies $\pi_n(\tilde{k}) > \pi_n(k)$, the achievable rate for the $\text{DU}_{n,\tilde{k}}$ to detect the $\text{DU}_{n,k}$'s signal is

$$\Gamma_i^u = \frac{p_i^u \left|\mathbf{a}_i^{ZF}\mathbf{h}_i^u\right|^2}{\sum\limits_{i'=1,i'\neq i}^{N_u} p_{i'}^u \left|\mathbf{a}_i^{ZF}\mathbf{h}_{i'}^u\right|^2 + \sum\limits_{n=1}^{N}\left|\sum\limits_{m'=1}^{M}\mathbf{a}_i^{ZF}\mathbf{G}_{m'}\mathbf{w}_{m',n}\right|^2 + \left|\mathbf{a}_i^{ZF}\mathbf{h}_{AP}^s\mathbf{w}_s\right|^2 + \sigma^2\left\|\mathbf{a}_i^{ZF}\right\|^2}. \quad (6)$$

$R_{n,\tilde{k}\to k} = \log_2\left(1+\Gamma^d_{n,\tilde{k}\to k}\right)$, where we have

$$\Gamma^d_{n,\tilde{k}\to k} = \frac{\sum\limits_{m=1}^{M} p_{n,k}\left|\mathbf{h}_{m,n,\tilde{k}}\mathbf{w}_{m,n}\right|^2}{\chi_{n,\tilde{k}}}, \quad (4)$$

where $\chi_{n,\tilde{k}}$ can be expressed as $\chi_{n,\tilde{k}} = \sum\limits_{n'\neq n}^{N}\left|\sum\limits_{m=1}^{M}\mathbf{h}_{m,n,\tilde{k}}\mathbf{w}_{m,n'}\right|^2 + \sum\limits_{i=1}^{N_u} p_i^u\left|g_{n,\tilde{k},i}\right|^2 + \left|\mathbf{h}^{st}_{n,\tilde{k}}\mathbf{w}_s\right|^2 + \sum\limits_{\pi_n(l)>\pi_n(k)} p_{n,l}\left|\sum\limits_{m=1}^{M}\mathbf{h}_{m,n,\tilde{k}}\mathbf{w}_{m,n}\right|^2 + \sigma^2$.

Remark 2. Equation (2) is the signal model relying on perfect SIC, while the residual interference of previously detected signals has to be considered for realistic imperfect SIC[1].

2) UL Transmission in Cell-free Systems: Due to spectrum sharing and the FD scheme, the UL signals received by the AP_m include the UUs' signals, the DL signals transmitted by the APs, the SI of the AP_m and the satellite DL signals. The UL signal received by the AP_m can be expressed as

$$\mathbf{y}_m^u = \sum_{i=1}^{N_u}\sqrt{p_i^u}\mathbf{h}_{m,i}^u s_i^u + \sum_{m'=1}^{M}\sum_{n=1}^{N}\mathbf{G}_{m,m'}\mathbf{w}_{m',n}s_n + \mathbf{h}^s_{AP_m}\mathbf{w}_s s_{sat} + \mathbf{n}_m, \quad (5)$$

where p_i^u is the transmit power of the UU_i, $\mathbf{h}_{m,i}$ is the channel vector between the UU_i and the AP_m, $\mathbf{G}_{m,m'} \in \mathbb{C}^{L_m\times L_{m'}}$ denotes the channel between the AP_m and the $\text{AP}_{m'}$, $\mathbf{h}^s_{AP_m}$ is the channel between the satellite and the AP_m, while $\mathbf{n}_m$ denotes the AWGN.

Given the received vector $\mathbf{a}$ at the AP_m, the UU_i's signal received by the AP_m can be expressed as $r^u_{m,i} = \mathbf{a}_{m,i}\mathbf{y}^u_m$, and the final aggregate received signal can be expressed as $r_i^u = \sum\limits_{m=1}^{M} r^u_{m,i}$. When employing the popular zero forcing (ZF) detection at the APs, the achievable rate of the UU_i is $R_i = \log_2(1+\Gamma_i^u)$, where Γ_i^u can be expressed as (6), where we have $\mathbf{a}_i^{ZF} \triangleq \left[\mathbf{a}_{1,i}^{ZF},...,\mathbf{a}_{M,i}^{ZF}\right] \in \mathbb{C}^{1\times L}$, $\mathbf{h}_i^u \triangleq \left[{\mathbf{h}_{1,i}^u}^T,...,{\mathbf{h}_{M,i}^u}^T\right]^T \in \mathbb{C}^{L\times 1}$, and $\mathbf{G}^T_{m'} \triangleq \left[\mathbf{G}^T_{1,m'}\cdots\mathbf{G}^T_{M,m'}\right]^T \in \mathbb{C}^{L\times L_{m'}}$.

3) DL Signal Transmission of the Satellite: The satellite broadcasts the same signal s_{sat} in its DL to all the SUs in a beam, where s_{sat} satisfies $\mathbb{E}\left[\left|s_{sat}\right|^2\right] = 1$. The received signal of the SU_j can be expressed as

$$y_j^s = \underbrace{\mathbf{h}_j^s\mathbf{w}_s s_{sat}}_{\text{desired signal}} + \underbrace{\sum_{m=1}^{M}\sum_{n=1}^{N}\mathbf{h}_{m,j}\mathbf{w}_{m,n}s_n + \sum_{i=1}^{N_u}\sqrt{p_i^u}h_{i,j}s_i^u}_{\text{INI}} + n_j, \quad (7)$$

where $\mathbf{h}_j^s \in \mathbb{C}^{1\times N_s}$ represents the channel between the satellite and the SU_j, $\mathbf{w}_s \in \mathbb{C}^{N_s\times 1}$ denotes the satellite's beamforming vector, $\mathbf{h}_{m,j} \in \mathbb{C}^{1\times L_m}$ is the channel between the AP_m and the SU_j, $h_{i,j}$ denotes the channel between the UU_i and the SU_j, while $n_j \sim \mathcal{CN}\left(0,\sigma_s^2\right)$ is the AWGN having the noise variance of σ_s^2. Hence, the achievable rate of the SU_j can be expressed as $R_j = \log_2(1+\Gamma_j)$, where we have

$$\Gamma_j = \frac{\left|\mathbf{h}_j^s\mathbf{w}_s\right|^2}{\sum\limits_{n=1}^{N}\left|\sum\limits_{m=1}^{M}\mathbf{h}_{m,j}\mathbf{w}_{m,n}\right|^2 + \sum\limits_{i=1}^{N_u}p_i^u|h_{i,j}|^2 + \sigma_s^2}. \quad (8)$$

IV. Problem Formulation

Based on the signal transmission model of Section III-A, we formulate our sum-rate maximization problem by jointly optimizing the power allocation of the NOMA DL, the transmit power of the UL, and the beamformer of both the APs and of the satellite as:

$$\max_{\substack{\mathbf{w},\mathbf{p},\\ \mathbf{p}^u,\mathbf{w}_s}} \sum_{n=1}^{N}\sum_{k=1}^{K}\log_2\left(1+\Gamma^d_{n,k\to k}\right) + \sum_{i=1}^{N_u}\log_2\left(1+\Gamma_i^u\right) \quad (9a)$$

$$\text{s.t.} \quad \sum_{n=1}^{N}\left\|\mathbf{w}_{m,n}\right\|^2 \le P_{AP}^{\max},\ \forall m, \quad (9b)$$

$$\left\|\mathbf{w}_s\right\|^2 \le P_s, \quad (9c)$$

$$\sum_{k=1}^{K} p_{n,k} = 1,\ \forall n, \quad (9d)$$

$$0 < p_{n,k} < 1, \forall n,k, \quad (9e)$$

$$0 \le p_i^u \le P_u^{\max},\ \forall i, \quad (9f)$$

$$\left|\sum_{m=1}^{M}\mathbf{h}_{m,n,\tilde{k}}\mathbf{w}_{m,n}\right|^2 \ge \left|\sum_{m=1}^{M}\mathbf{h}_{m,n,k}\mathbf{w}_{m,n}\right|^2, \quad \text{if } \pi_n(\tilde{k}) > \pi_n(k), \forall n,k, \quad (9g)$$

$$\log_2\left(1+\Gamma^d_{n,\tilde{k}\to k}\right) \ge \log_2\left(1+\Gamma^d_{n,k\to k}\right), \quad \text{if } \pi_n(\tilde{k}) > \pi_n(k),\ \forall n,k, \quad (9h)$$

$$\log_2\left(1+\Gamma^d_{n,k\to k}\right) \ge \gamma^d_{n,k},\ \forall n,k, \quad (9i)$$

$$\log_2\left(1+\Gamma_i^u\right) \ge \gamma_i^u,\ \forall i, \quad (9j)$$

$$\log_2\left(1+\Gamma_j\right) \ge \gamma_j,\ \forall j, \quad (9k)$$

[1]For the imperfect SIC, we have $\chi_{m,n,k} = \sum\limits_{\pi_n(\tilde{l})<\pi_n(k)}\delta_{\tilde{l}}\left|\sum\limits_{m=1}^{M}\mathbf{h}_{m,n,k}\mathbf{w}_{m,n}\right|^2 + \sum\limits_{\pi_n(l)>\pi_n(k)}p_{n,l}\left|\sum\limits_{m=1}^{M}\mathbf{h}_{m,n,k}\mathbf{w}_{m,n}\right|^2 + \sum\limits_{n'\neq n}\left|\sum\limits_{m=1}^{M}\mathbf{h}_{m,n,k}\mathbf{w}_{m,n'}\right|^2 + \sum\limits_{i=1}^{N_u}p_i^u|g_{n,k,i}|^2 + \left|\mathbf{h}^{st}_{n,k}\mathbf{w}_s\right|^2 + \sigma^2$, where the first term is the residual interference of the previously detected NOMA users due to the imperfect SIC.

$$\Gamma_{n,k\to k}^{d}=\frac{p_{n,k}\mathrm{Tr}\left(\mathbf{H}_{n,k}\mathbf{W}_{n}\right)}{\sum\limits_{\pi_n(l)>\pi_n(k)}p_{n,l}\mathrm{Tr}\left(\mathbf{H}_{n,k}\mathbf{W}_{n}\right)+\sum\limits_{n'\neq n}\mathrm{Tr}\left(\mathbf{H}_{n,k}\mathbf{W}_{n'}\right)+\mathrm{Tr}\left(\mathbf{p}^{u}\mathbf{G}_{n,k}\right)+\mathrm{Tr}\left(\mathbf{H}_{n,k}^{st}\mathbf{W}_{s}\right)+\sigma^{2}}. \tag{10}$$

$$\Gamma_{n,\tilde{k}\to k}^{d}=\frac{p_{n,k}\mathrm{Tr}\left(\mathbf{H}_{n,\tilde{k}}\mathbf{W}_{n}\right)}{\sum\limits_{\pi_n(l)>\pi_n(k)}p_{n,l}\mathrm{Tr}\left(\mathbf{H}_{n,\tilde{k}}\mathbf{W}_{n}\right)+\sum\limits_{n'\neq n}\mathrm{Tr}\left(\mathbf{H}_{n,\tilde{k}}\mathbf{W}_{n'}\right)+\mathrm{Tr}\left(\mathbf{p}^{u}\mathbf{G}_{n,\tilde{k}}\right)+\mathrm{Tr}\left(\mathbf{H}_{n,\tilde{k}}^{st}\mathbf{W}_{s}\right)+\sigma^{2}}. \tag{11}$$

where $\mathbf{w}$ is the DL beamforming matrix of all the APs, $\mathbf{p}$ is the power allocation factor matrix of the NOMA DL, $\mathbf{p}^u$ is the UL transmit power matrix of all the UUs, and $\mathbf{w}_s$ is the satellite's beamforming vector. Furthermore, (9b) denotes the beamforming design of the APs, which implies that the transmit power of each AP is limited by the maximum power budgets $P_{AP}^{\max}$, (9c) represents the relationship of beamforming and the power control of the satellite, where P_s denotes the total power of the satellite. To expound further, (9d) and (9e) denote the power allocation constraints of the NOMA DL, (9f) is the transmit power constraint of the UUs, (9g) is to guarantee the higher channel gain of the $\tilde{k}$-th user once we define the $\tilde{k}$-th user is detected after the k-th user, hence maintaining the fairness with the given SIC order. (9h) is to guarantee that the SIC can be carried out, and finally, (9i)-(9k) are used for guaranteeing the minimal required rate of the DUs, of the UUs, and of the SUs, where $\gamma_{n,k}^{d}$, γ_i^u and γ_j denote their minimal required rates, respectively.

V. Proposed Joint Optimization Design

In this section, we develop a joint beamforming and power allocation design for addressing the non-convexity of problem (9) by employing SCA and SDP methods. To find a sub-optimal solution, we first transform (9) into an equivalent SDP problem with rank-one constraints. Upon defining $\mathbf{W}_n=\mathbf{w}_n\mathbf{w}_n^{\dagger}$ and $\mathbf{W}_s=\mathbf{w}_s\mathbf{w}_s^{\dagger}$, where $\mathbf{w}_n=[\mathbf{w}_{1,n}^T,...,\mathbf{w}_{m,n}^T]^T\in\mathbb{C}^{L\times 1}$ denotes the beamforming vector for the n-th cluster of all APs. Note that $\mathbf{W}_n$ and $\mathbf{W}_s$ have to be rank-one positive semi-definite (PSD) matrices, i.e., $\mathbf{W}_n\succeq\mathbf{0}$, $\mathbf{W}_s\succeq\mathbf{0}$, and $\mathrm{Rank}\left(\mathbf{W}_n\right)=1$, $\mathrm{Rank}\left(\mathbf{W}_s\right)=1$. Therefore, $\Gamma_{n,k\to k}^{d}$ can be expressed as (10), where we have $\mathbf{h}_{n,k}=[\mathbf{h}_{1,n,k},...,\mathbf{h}_{M,n,k}]\in\mathbb{C}^{1\times L}$, $\mathbf{p}^u=\mathrm{diag}(p_1^u,...,p_{N_u}^u)$, $\mathbf{g}_{n,k}=[g_{n,k,1},...,g_{n,k,N_u}]$. Furthermore, $\mathbf{H}_{n,k}=\mathbf{h}_{n,k}^{\dagger}\mathbf{h}_{n,k}\in\mathbb{C}^{L\times L}$, $\mathbf{G}_{n,k}=\mathbf{g}_{n,k}^{\dagger}\mathbf{g}_{n,k}$, and $\mathbf{H}_{n,k}^{st}=(\mathbf{h}_{n,k}^{st})^{\dagger}\mathbf{h}_{n,k}^{st}$. Similarly, $\Gamma_{n,\tilde{k}\to k}^{n}$ in (9h) can be expressed as (11). Furthermore, Γ_i^u and Γ_j can be reformulated as in (12) and (13).

$$\Gamma_{i}^{u}=\frac{p_{i}^{u}\eta_{i,i}}{\sum\limits_{i'\neq i}p_{i}^{u}\eta_{i,i'}+\sum\limits_{n=1}^{N}\mathrm{Tr}(\tilde{\mathbf{A}}\mathbf{W}_{n})+\mathrm{Tr}(\hat{\mathbf{A}}\mathbf{W}_{s})+\sigma^{2}\left\|\mathbf{a}_{i}^{ZF}\right\|^{2}}, \tag{12}$$

$$\Gamma_{j}=\frac{\mathrm{Tr}(\mathbf{H}_{j}^{s}\mathbf{W}_{s})}{\sum\limits_{n=1}^{N}\mathrm{Tr}\left(\mathbf{H}_{j}\mathbf{W}_{n}\right)+\sum\limits_{i=1}^{N_u}p_{i}^{u}|h_{i,j}|^{2}+\sigma_{s}^{2}}, \tag{13}$$

where in (12), we have $\eta_{i,i}=\left|\mathbf{a}_i^{ZF}\mathbf{h}_i^u\right|^2$, $\eta_{i,i'}=\left|\mathbf{a}_i^{ZF}\mathbf{h}_{i'}^u\right|^2(i'\neq i)$, $\tilde{\mathbf{a}}=\mathbf{a}_i^{ZF}\mathbf{G}$, and $\hat{\mathbf{a}}=\mathbf{a}_i^{ZF}\mathbf{h}_{AP}^s$. Furthermore, we have $\tilde{\mathbf{A}}=\tilde{\mathbf{a}}^{\dagger}\tilde{\mathbf{a}}\in\mathbb{C}^{L\times L}$, and $\hat{\mathbf{A}}=\hat{\mathbf{a}}^{\dagger}\hat{\mathbf{a}}$. In (13), we have $\mathbf{H}_j^s=(\mathbf{h}_j^s)^{\dagger}\mathbf{h}_j^s$, and $\mathbf{H}_j=\mathbf{h}_j^{\dagger}\mathbf{h}_j$, where $\mathbf{h}_j=[\mathbf{h}_{1,j},...,\mathbf{h}_{M,j}]\in\mathbb{C}^{1\times L}$.

Then the optimization problem (9) can be reformulated as

$$\max_{\substack{\mathbf{w},\mathbf{p},\\ \mathbf{p}^u,\mathbf{w}_s}}\ \sum_{n=1}^{N}\sum_{k=1}^{K}\log_2\left(1+\Gamma_{n,k\to k}^{d}\right)+\sum_{i=1}^{N_u}\log_2\left(1+\Gamma_i^u\right) \tag{14a}$$

$$\text{s.t.}\quad \mathrm{Rank}\left(\mathbf{W}_n\right)=1,\forall n, \tag{14b}$$

$$\mathrm{Rank}\left(\mathbf{W}_s\right)=1, \tag{14c}$$

$$\sum_{n=1}^{N}\mathrm{Tr}\left([\mathbf{W}_n]_m\right)\leq P_{AP}^{\max},\forall m, \tag{14d}$$

$$\mathrm{Tr}\left(\mathbf{W}_s\right)\leq P_s, \tag{14e}$$

$$\mathbf{W}_n\succeq\mathbf{0},\forall n, \tag{14f}$$

$$\mathbf{W}_s\succeq\mathbf{0}, \tag{14g}$$

$$\mathrm{Tr}\left(\mathbf{H}_{n,\tilde{k}}\mathbf{W}_n\right)\geq\mathrm{Tr}\left(\mathbf{H}_{n,k}\mathbf{W}_n\right),\ \text{if}\ \pi_n(\tilde{k})>\pi_n(k), \tag{14h}$$

$$\text{(9d)}-\text{(9f)},\text{(9h)}-\text{(9k)}, \tag{14i}$$

where $[\mathbf{W}_n]_m\in\mathbb{C}^{L_m\times L_m}$ denotes elements between the $[(m-1)L_m+1,(m-1)L_m+1]$-th element and $[mL_m,mL_m]$-th element in $\mathbf{W}_n$.

Remark 3. The optimization problem (14) is equivalent to the original problem if and only if the rank-one constraint is satisfied. When the rank-one constraint is guaranteed, the vectorial solution of (9) can be retrieved from the matrix solution of (14). However, even if the rank-one constraint is satisfied, the objective function (14a) and constraints (9h)-(9k) are still non-convex.

We first tackle the non-convex nature of the objective function (14a). The first term of (14a) can be reformulated as $\sum\limits_{n=1}^{N}\sum\limits_{k=1}^{K}\log_2 e\ln\left(\frac{(p_{n,k}+\sum\limits_{\pi_n(l)>\pi_n(k)}p_{n,l})\mathrm{Tr}(\mathbf{H}_{n,k}\mathbf{W}_n)+\phi_{n,k}}{\sum\limits_{\pi_n(l)>\pi_n(k)}p_{n,l}\mathrm{Tr}(\mathbf{H}_{n,k}\mathbf{W}_n)+\phi_{n,k}}\right)$, where we have $\phi_{n,k}=\mathrm{Tr}\left(\mathbf{p}^u\mathbf{G}_{n,k}\right)+\sum\limits_{n'\neq n}\mathrm{Tr}\left(\mathbf{H}_{n,k}\mathbf{W}_{n'}\right)+\mathrm{Tr}\left(\mathbf{H}_{n,k}^{st}\mathbf{W}_s\right)+\sigma^2$. Then, we introduce a set of auxiliary variables $\{x_{n,k}\}$, $\{y_{n,k}\}$ to relax the numerator and denominator so that we have [25]

$$e^{x_{n,k}}\leq(p_{n,k}+\sum_{\pi_n(l)>\pi_n(k)}p_{n,l})\mathrm{Tr}\left(\mathbf{H}_{n,k}\mathbf{W}_n\right)+\phi_{n,k}, \tag{15}$$

$$e^{y_{n,k}}\geq\sum_{\pi_n(l)>\pi_n(k)}p_{n,l}\mathrm{Tr}\left(\mathbf{H}_{n,k}\mathbf{W}_n\right)+\phi_{n,k}. \tag{16}$$

Therefore, the first term of (14a) can be then formulated as the convex linear expression $\log_2 e \sum_{n=1}^{N}\sum_{k=1}^{K}(x_{n,k}-y_{n,k})$. Similarly, we introduce another set of auxiliary variables $\{x_i\}$ and $\{y_i\}$ to transform the second term of (14a) into the linear expression of $\log_2 e \sum_{i=1}^{N_u}(x_i - y_i)$ as

$$e^{x_i} \leq \sum_{i'=1}^{N_u} p_{i'}^u \eta_{i,i'} + \sum_{n=1}^{N} \mathrm{Tr}(\tilde{\mathbf{A}}\mathbf{W}_n) + \mathrm{Tr}(\hat{\mathbf{A}}\mathbf{W}_s) + \sigma^2 \left\|\mathbf{a}_i^{ZF}\right\|^2, \tag{17}$$

$$e^{y_i} \geq \sum_{i'\neq i} p_{i'}^u \eta_{i,i'} + \sum_{n=1}^{N} \mathrm{Tr}(\tilde{\mathbf{A}}\mathbf{W}_n) + \mathrm{Tr}(\hat{\mathbf{A}}\mathbf{W}_s) + \sigma^2 \left\|\mathbf{a}_i^{ZF}\right\|^2. \tag{18}$$

Then, the optimization problem can be reformulated as

$$\max_{\substack{\mathbf{W}_n,\mathbf{p},\\ \mathbf{p}^u,\mathbf{W}_s}} \quad \log_2 e \sum_{n=1}^{N}\sum_{k=1}^{K}(x_{n,k}-y_{n,k}) + \log_2 e \sum_{i=1}^{N_u}(x_i - y_i) \tag{19a}$$

$$\text{s.t.} \quad (14b)-(14i), (15)-(18). \tag{19b}$$

In (19), the objective function (19a) is convex after introducing new non-convex constraints (15), (16), and (18). We first replace the constraint (15) by the following relaxed convex constraints by using the S-Procedure method [42] as

$$\mathbf{Q}_{n,k} \triangleq \begin{bmatrix} p_{n,k} + \sum\limits_{\pi_n(l)>\pi_n(k)} p_{n,l} & \lambda_{n,k} \\ \lambda_{n,k} & \mathrm{Tr}\left(\mathbf{H}_{n,k}\mathbf{W}_n\right) \end{bmatrix} \succeq \mathbf{0}, \tag{20}$$

$$e^{x_{n,k}} \leq \tilde{\lambda}_{n,k}\lambda_{n,k} - \tilde{\lambda}_{n,k}^2 + \phi_{n,k}, \tag{21}$$

where the right-hand-side of (21) follows from the lower bound obtained by the first-order Taylor expansion of $\lambda_{n,k}^2$ at the feasible point $\tilde{\lambda}_{n,k}$. Given the constraint (16), since $e^{y_{n,k}}$ is convex with respect to $y_{n,k}$, its linearized lower bound at the given point $\tilde{y}_{n,k}$ is given by

$$e^{y_{n,k}} \geq e^{\tilde{y}_{n,k}}\left(y_{n,k} - \tilde{y}_{n,k} + 1\right). \tag{22}$$

We then further introduce the variables $\{a_{n,k}\}$ to address the multiplication of variables in the right-hand-side of (16) such that

$$e^{\tilde{y}_{n,k}}\left(y_{n,k} - \tilde{y}_{n,k} + 1\right) \geq a_{n,k}^2 + \phi_{n,k}, \tag{23}$$

where $\{a_{n,k}\}$ should satisfy

$$a_{n,k}^2 \geq \sum_{\pi_n(l)>\pi_n(k)} p_{n,l}\mathrm{Tr}\left(\mathbf{H}_{n,k}\mathbf{W}_n\right). \tag{24}$$

Furthermore, by introducing slack variables $\{b_{n,k}\}$ so that

$$b_{n,k} \geq \mathrm{Tr}\left(\mathbf{H}_{n,k}\mathbf{W}_n\right), \tag{25}$$

the non-convex constraint (24) can be further replaced by

$$\sum_{\pi_n(l)>\pi_n(k)} p_{n,l} \leq \frac{\tilde{a}_{n,k}^2}{\tilde{b}_{n,k}} + \frac{2\tilde{a}_{n,k}\left(a_{n,k}-\tilde{a}_{n,k}\right)}{\tilde{b}_{n,k}} - \frac{\tilde{a}_{n,k}^2\left(b_{n,k}-\tilde{b}_{n,k}\right)}{\tilde{b}_{n,k}^2}. \tag{26}$$

Due to the convexity of the function $f(x,y) \triangleq \frac{x^2}{y}$ with respect to x and y with $(x,y) \in \mathbb{R}^{++}$, the right-hand-side of (26) denotes the lower bound of $\frac{b_{n,k}^2}{a_{n,k}}$ obtained by the first-order Taylor expansion at the feasible point $(\tilde{a}_{n,k}, \tilde{b}_{n,k})$. Furthermore, (18) can be transformed into

$$e^{\tilde{y}_i}\left(y_i - \tilde{y}_i + 1\right) \geq \sum_{i'\neq i} p_{i'}^u \eta_{i,i'} + \sum_{n=1}^{N} \mathrm{Tr}(\tilde{\mathbf{A}}\mathbf{W}_n) + \mathrm{Tr}(\hat{\mathbf{A}}\mathbf{W}_s) + \sigma^2 \left\|\mathbf{a}_i^{ZF}\right\|^2, \tag{27}$$

where $\tilde{y}_i$ is the Taylor expansion's feasible point. Then the optimization problem (19) can be reformulated as

$$\max_{\substack{\mathbf{W}_n,\mathbf{p},\mathbf{p}^u,\mathbf{W}_s,\\ x_{n,k},y_{n,k},x_i,y_i}} \quad \log_2 e \sum_{n=1}^{N}\sum_{k=1}^{K}(x_{n,k}-y_{n,k}) + \sum_{i=1}^{N_u}(x_i - y_i) \tag{28a}$$

$$\text{s.t.} \quad (14b)-(14i), (17), (20), (21), (23), (25)-(27). \tag{28b}$$

However, problem (28) is still non-convex due to the constraints (9h)−(9k). We first relax (9h) as $\log_2\left(1+\Gamma_{n,\tilde{k}\to k}^d\right) \geq \bar{\gamma}$, which indicates that the SIC can be performed when the achievable rate for the $\mathrm{DU}_{n,\tilde{k}}$ to detect the $\mathrm{DU}_{n,k}$'s signal is higher than the threshold $\bar{\gamma}$. Therefore, (9h) can be reformulated as

$$(p_{n,k} - \bar{\zeta}\sum_{\pi_n(l)>\pi_n(k)} p_{n,l})\mathrm{Tr}\left(\mathbf{H}_{n,\tilde{k}}\mathbf{W}_n\right) - \bar{\zeta}\phi_{n,\tilde{k}} \geq 0, \tag{29}$$

where $\bar{\zeta} = (2^{\bar{\gamma}} - 1)$. Upon recalling the S-procedure, (29) can be replaced by the following convex constraints

$$\begin{bmatrix} p_{n,k} - \bar{\zeta}\sum\limits_{\pi_n(l)>\pi_n(k)} p_{n,l} & \varsigma_{n,k}^{\tilde{k}} \\ \varsigma_{n,k}^{\tilde{k}} & \mathrm{Tr}\left(\mathbf{H}_{n,\tilde{k}}\mathbf{W}_n\right) \end{bmatrix} \succeq \mathbf{0}, \tag{30}$$

$$\tilde{\varsigma}_{n,k}^{\tilde{k}}\varsigma_{n,k}^{\tilde{k}} - (\varsigma_{n,k}^{\tilde{k}})^2 - (2^{\bar{\gamma}}-1)\phi_{n,\tilde{k}} \geq 0, \ \pi_n(\tilde{k}) > \pi_n(k), \tag{31}$$

where the left-hand-side of (31) comes from the first-order Taylor expansion of $(\varsigma_{n,k}^{\tilde{k}})^2$ at the feasible point $\tilde{\varsigma}_{n,k}^{\tilde{k}}$. Similarly, (9i) can be replaced by the following convex constraints:

$$\begin{bmatrix} p_{n,k} - (2^{\gamma_{n,k}^d}-1)\sum\limits_{\pi_n(l)>\pi_n(k)} p_{n,l} & \varsigma'_{n,k} \\ \varsigma'_{n,k} & \mathrm{Tr}\left(\mathbf{H}_{n,k}\mathbf{W}_n\right) \end{bmatrix} \succeq \mathbf{0}, \tag{32}$$

$$\tilde{\varsigma}'_{n,k}\varsigma_{n,k} - (\tilde{\varsigma}'_{n,k})^2 - (2^{\gamma_{n,k}^d}-1)\phi_{n,k} \geq 0. \tag{33}$$

For constraints (9j) and (9k), we can readily obtain their

equivalent convex expressions as

$$p_i^u\eta_{i,i} - (2^{\gamma_i^u}-1)\left(\sum_{i'\neq i} p_{i'}^u\eta_{i,i'} + \sum_{n=1}^{N}\mathrm{Tr}(\tilde{\mathbf{A}}\mathbf{W}_n)\right) - (2^{\gamma_i^u}-1)\left(\mathrm{Tr}(\hat{\mathbf{A}}\mathbf{W}_s) + \sigma^2\left\|\mathbf{a}_i^{ZF}\right\|^2\right) \geq 0, \tag{34}$$

and

$$\mathrm{Tr}(\mathbf{H}_j^s\mathbf{W}_s) - (2^{\gamma_j}-1)\left(\sum_{n=1}^{N}\mathrm{Tr}\left(\mathbf{H}_j\mathbf{W}_n\right) + \sum_{i=1}^{N_u} p_i^u|h_{i,j}|^2\right) - (2^{\gamma_j}-1)\sigma_s^2 \geq 0. \tag{35}$$

Based on the aforementioned transformations and approximations, all the constraints can be approximated by convex constraints and the rank-one constraints can be provably satisfied. Hence, we drop the rank-one constraint in order to obtain a relaxed version. We finally arrive at the following convex problem, which can be solved efficiently by off-the-shelf solvers.

$$\max_{\mathbf{\Phi}} \ \log_2 e\sum_{n=1}^{N}\sum_{k=1}^{K}(x_{n,k}-y_{n,k}) + \sum_{i=1}^{N_u}(x_i - y_i) \tag{36a}$$

$$\text{s.t.} \quad \begin{array}{l}(9\text{d})-(9\text{f}),(14\text{d})-(14\text{h}),(17),(20),(21),(23),\\ (25)-(27),(30)-(35),\end{array} \tag{36b}$$

where $\mathbf{\Phi} \triangleq \{\mathbf{W}_n, \mathbf{W}_s, p_{n,k}, p_i^u, x_{n,k}, y_{n,k}, x_i, y_i, \lambda_{n,k}, a_{n,k}, b_{n,k}, \varsigma_{n,k}^{\tilde{k}}, \varsigma_{n,k}'\}$ defines the optimization variables, and $\tilde{\mathbf{\Phi}} \triangleq \{\tilde{y}_{n,k}, \tilde{y}_i, \tilde{\lambda}_{n,k}, \tilde{a}_{n,k}, \tilde{b}_{n,k}, \tilde{\varsigma}_{n,k}^{\tilde{k}}, \tilde{\varsigma}_{n,k}'\}$ is the feasible set updated after each iteration. Finally, the proposed jointly optimized beamforming and optimal power (OBOP) allocation procedure is summarized in **Algorithm 1**. The proof of its relaxed rank-one constraint, its convergence and complexity discussions are given as follows.

Remark 4. In our proposed algorithm, an inappropriate initial set $\tilde{\mathbf{\Phi}}^{(0)}$ may lead to a heavy computational complexity and infeasibility of the proposed algorithm. The feasible initialization of $\tilde{\mathbf{\Phi}}^{(0)}$ can be obtained by the algorithm in [25].

Remark 5. For the beamforming vector $\mathbf{w}_n$ obtained, $\mathbf{w}_n\left[(m-1)L_m+1 : mL_m\right]$ denotes the beamforming vector used for the n-th NOMA cluster at the m-th AP.

Theorem 1. *The optimal solutions $\mathbf{W}_n^*$ and $\mathbf{W}_s^*$ obtained are always rank-one matrices, despite the relaxation of the rank constraint. The proof is similar to that in [42], hence we omit it for brevity.*

A. Convergence Analysis

We define the obtained solution and the feasible point of (36) at the κ-th iteration as $\mathbf{\Phi}^{(\kappa)}$ and $\tilde{\mathbf{\Phi}}^{(\kappa)}$. Due to the form of objective function of (36), we have $y_{n,k}^{\kappa} \leq \tilde{y}_{n,k}^{\kappa}$. Furthermore, according to [25], we have

$$\begin{aligned} e^{\tilde{y}_{n,k}^{(\kappa+1)}} &= \sum_{\pi_n(l)>\pi_n(k)} p_{n,l}^{(\kappa)}\mathrm{Tr}\left(\mathbf{H}_{n,k}\mathbf{W}_n^{(\kappa)}\right) + \phi_{n,k}^{(\kappa)} \\ &\leq e^{\tilde{y}_{n,k}^{(\kappa)}}\left(y_{n,k}^{(\kappa)} - \tilde{y}_{n,k}^{(\kappa)} + 1\right) \overset{(a)}{\leq} e^{y_{n,k}^{(\kappa)}}, \end{aligned} \tag{37}$$

Algorithm 1: Jointly optimized beamforming and optimal power (OBOP) allocation algorithm

Initialization: Set the randomly distributed APs and users;
Generate channels $\mathbf{h}_{m,n,k}$, $\mathbf{h}_{n,k}^{st}$, $\mathbf{h}_{m,i}$, $\mathbf{h}_{AP_m}^s$, $\mathbf{h}_j^s$, $\mathbf{h}_{m,j}$, $\mathbf{G}_{m,m'}$, $h_{i,j}$, $g_{n,k,i}$;
Set the tolerance of iteration accuracy $\tilde{\delta}$, the max iteration time I_{max}, the initial iteration index $\kappa = 0$, and the initial set $\tilde{\mathbf{\Phi}}^{(0)}$;
while $\kappa \leq I_{max}$ *and* $\hat{\delta} > \tilde{\delta}$ **do**
  $\kappa = \kappa + 1$;
  Solve (36) to obtain the solution $\mathbf{\Phi}^{(\kappa)}$ and the obhective value $\mathcal{F}^{(\kappa)}$;
  Update $\tilde{\mathbf{\Phi}}^{(\kappa)}$ by the obtained solution $\mathbf{\Phi}^{(\kappa)}$ similar as [25] ;
  Update the iteration accuarcy $\hat{\delta} = \left|\mathcal{F}^{(\kappa)} - \mathcal{F}^{(\kappa-1)}\right|$;
end
Using singular value decomposition (SVD) to $\mathbf{W}_n^{(\kappa)}$ and $\mathbf{W}_s^{(\kappa)}$ to obtain $\mathbf{w}_n$ and $\mathbf{w}_s$;
Output: Beamforming vectors at APs and the satellite, UL transmit power of UUs, power allocation factors of NOMA users.

where (a) holds due to the first-order Taylor expansion. Hence it may be readily shown that $\tilde{y}_{n,k}^{(\kappa+1)} \leq y_{n,k}^{(\kappa)}$.

Furthermore, we have $\sigma^2 \leq e^{\tilde{y}_{n,k}^{(\kappa)}} \leq \infty$. Therefore, $y_{n,k}^{(\kappa)}$ is a bounded monotonic function and converges as the iteration index κ increases. Meanwhile, we have $\tilde{y}_{n,k}^{(\kappa+1)} \leq y_{n,k}^{\kappa} \leq \tilde{y}_{n,k}^{(\kappa)}$, hence $y_{n,k}^{(\kappa)}$ also converges. Similarly, we have

$$e^{\tilde{y}_i^{(\kappa+1)}} \leq e^{\tilde{y}_i^{(\kappa)}}\left(y_i^{(\kappa)} - \tilde{y}_i^{(\kappa)} + 1\right) \leq e^{y_i^{(\kappa)}}, \tag{38}$$

Similarly, $y_i^{(\kappa)}$ and $\tilde{y}_i^{(\kappa)}$ are guaranteed to be converged. Our proposed algorithm is guaranteed to converge.

B. Complexity Analysis

Observe that the complexity of our proposed algorithm depends on the SDP procedure, whose complexity is $\mathcal{O}\left[I_{\max}\left(m_{sdp}n_{sdp}^{3.5} + m_{sdp}^2 n_{sdp}^{2.5} + m_{sdp}^3 n_{sdp}^{0.5}\right)\right]$, where m_{sdp} is the number of semidefinite constraints, n_{sdp} denotes the dimension of semidefinite cone and $I_{\max}$ is the number of iterations. To find the optimal SIC order, the complexity of exhaustively searching all possible combinations is $\mathcal{O}[N(K!)]$, and the complexity of our proposed SIC order checking is $\mathcal{O}(1)$.

VI. Simulation Results

In this section, we provide representative simulation results for quantifying the performance of our proposed algorithm, when relying on realistic imperfect SIC and imperfect channel estimation. The simulation parameters without specific definitions are summarized at a glance in Table III. The satellite channel and terrestrial channel models are given as follows.

A. Channel Setups

1) Satellite Channel: The satellite channel is characterized in terms of its large-scale and small-scale fading. The instantaneous free-space path-loss is expressed as $C_L = \left(\frac{c}{4\pi f_c d_s}\right)^2$,

and the power of noise σ_s^2 can be expressed as $\sigma_s^2 = K_B T W$ [43]. Ih these equations, K_B is the Boltzman constant, $K_B = 1.38\times10^{-23}$ J/K, T is the receiver's noise temperature, c is the speed of light, W is the carrier's bandwidth, f_c is the carrier frequency, and d_s is the distance between the satellite and the terrestrial components, which can be further expressed as $d_s = d_h^2 + d_u^2$, where d_h is the satellite's altitude and d_u is the distance from the beam's center to the terrestrial components.

Moreover, we consider another satellite-terrestrial channel model, namely that used in 3GPP TR 38.811 [44]. The signal suffers from the following path-loss

$$PL = PL_b + PL_g + PL_s + PL_e, \tag{39}$$

where PL is the total path loss, PL_b is the propagation path loss, PL_g is the attenuation due to atmospheric gasses, PL_s is the attenuation due to either ionospheric or tropospheric scintillation, and PL_e is the building penetration loss. For the simplicity, we only consider the propagation path loss PL_b as well as the rain and cloud attenuation formulated as

$$C_L = PL_b + a_{rain}, \tag{40}$$

where we have $PL_b = FSPL(d_s, f_c) + SF + C_{cl}(\alpha, f_c)$, $FSPL(d_s, f_c) = 32.45 + 20\log_{10}(f_c) + 20\log_{10}(d_s)$, SF is the shadow fading loss represented by a random number generated by the normal distribution, i.e., $SF \sim N\left(0, \sigma_{SF}^2\right)$, and $C_{cl}(\alpha, f_c)$ is the clutter loss. The value of σ_{SF}^2 and $C_{cl}(\alpha, f_c)$ can be found in [44]. We set these parameters to $\sigma_{SF}^2 = 4$dB, $C_{cl}(\alpha, f_c) = 33$dB, respectively. Furthermore, the rain attenuation a_{rain} varies with the rainfall intensity. Specifically, the rainfall can be clarified into light rain, moderate rain, and heavy rain, whose rainfall intensity is 1 mm/hour, 4 mm/hour, and 16 mm/hour. The corresponding rain attenuation value a_{rain} is 1.5dB, 5.6dB, and 16dB, respectively [45].

The satellite's beam gain can be expressed as [43]

$$\vartheta(\theta) = \tilde{\vartheta}\left(\frac{J_1(\rho)}{2\rho} + 36\frac{J_3(\rho)}{\rho^3}\right), \tag{41}$$

where θ is the angular separation of the users from the satellite's beam center, $\tilde{\vartheta}$ is the antenna gain at the users, $J(\cdot)$ is the Bessel function, $\rho = 2.07123\frac{\sin\theta}{\sin\theta_{3\text{dB}}}$, and $\theta_{3\text{dB}}$ is the 3dB beam-width. The small-scale fading of satellite channels can be modeled by Shadowed-Rician fading [43].

2) Terrestrial Channel: The channel $\mathbf{G}_{m,m'}$ between any two APs m and m' can be modeled as [24]

$$\mathbf{G}_{m,m'} = \begin{cases} \sqrt{\rho_{SI}}\mathbf{G}_{m,m}^{SI}, \text{ if } m = m', \\ \mathbf{G}_{m,m'}^{AA}, \text{ otherwise}, \end{cases} \tag{42}$$

where $\mathbf{G}_{m,m}^{SI}$ denotes the SI channel which interferes with the receive of UL signals due to the co-current DL transmission at AP_m, $\mathbf{G}_{m,m'}^{AA}$ denotes the channel between any two different APs, while ρ_{SI} is the residual SI level after interference cancellation. Similar to [24], [46], we model $\mathbf{G}_{m,m}^{SI}$ by the Rician distribution having a low Rician factor, which is set to 0.1, while the other channels in the terrestrial layer are modeled by Rayleigh fading, and their large-scale path-loss can be formulated as [24]

$$\beta = 10^{\frac{PL(d)+\sigma_{sh}n_{sf}}{10}}, \tag{43}$$

where $n_{sf} \sim \mathcal{N}(0, \sigma_{sh})$ represents the shadow fading, σ_{sh} is the standard deviation of n_{sf} having the value of 8dB, and $PL(d)$ can be expressed as [24], [39]

$$\begin{aligned} PL(d) = &-140.7 - 35\log_{10}(d) + 20c_0\log_{10}\left(\frac{d}{d_0}\right) \\ &+ 15c_1\log_{10}\left(\frac{d}{d_1}\right), \end{aligned} \tag{44}$$

where d is the distance between transceivers, $c_i = \max\left\{0, \frac{d_i - d}{|d_i - d|}\right\}$, where d_i denotes the reference distance, $i \in \{0, 1\}$.

Furthermore, we consider the channel estimation in the cell-free system as follows.

3) Terrestrial Channel Estimation: To complete the channel estimation procedure, the terrestrial users first transmit their pilot signals to the APs before their signal transmission. Then the APs determine both the beamforming vectors as well as transmit power by relying on the estimated channels. In this part, first the channel estimation procedure is considered, followed by the derivation of the corresponding estimation error.

To be specific, the DUs and the UUs send their training sequences in different intervals[2]: in the first phase, the UUs send their pilots to the APs, while the DUs transmit their pilots to the APs during the second phase [24].

We assume that all the DUs simultaneously transmit their pilot sequences to the APs, and the pilot signal received at the AP_m is formulated as

$$\mathbf{Y}_m = \sqrt{\tau\tilde{p}_p}\sum_{n=1}^{N}\sum_{k=1}^{K}\mathbf{h}_{m,n,k}^T\boldsymbol{\varphi}_{n,k}^\dagger + \mathbf{N}_m, \tag{45}$$

where $\boldsymbol{\varphi}_{n,k} \in \mathbb{C}^{\tau\times1}$ is the pilot sequence of the $\text{DU}_{n,k}$ (the k-th DU in the n-th cluster), which satisfies $\|\boldsymbol{\varphi}_{n,k}\|^2 = 1$. Furthermore, τ is the length of pilot sequence[3], $\tilde{p}_p$ is the pilot's transmit power, $\mathbf{h}_{m,n,k} \in \mathbb{C}^{1\times L_m}$ is the channel between the $\text{DU}_{n,k}$ and the AP_m, and $\mathbf{N}_m \in \mathbb{C}^{L_m\times\tau}$ is the AWGN matrix obeying $\mathbf{N}_m \sim \mathcal{CN}\left(0, \sigma^2\mathbf{I}\right)$. Upon using the classic minimum mean-square error (MMSE) channel estimation [21], the estimated channel is given by

$$\hat{\mathbf{h}}_{m,n,k} = \frac{\sqrt{\tau\tilde{p}_p}\beta_{m,n,k}}{\sigma^2 + \tau\tilde{p}_p\sum\limits_{n'=1}^{N}\sum\limits_{k'=1}^{K}\beta_{m,n',k'}|\boldsymbol{\varphi}_{n,k}^\dagger\boldsymbol{\varphi}_{n',k'}|^2}\tilde{\mathbf{y}}_{m,n,k}, \tag{46}$$

where $\tilde{\mathbf{y}}_{m,n,k} = \mathbf{Y}_m\boldsymbol{\varphi}_{n,k}$, $\beta_{m,n,k}$ is the large-scale fading of the link between the AP_m and the $\text{DU}_{n,k}$. We denote the channel estimation error by $\delta_{m,n,k} = \mathbf{h}_{m,n,k} - \hat{\mathbf{h}}_{m,n,k}$, which follows $\delta_{m,n,k} \sim$

[2]Naturally, the slots used for pilot transmission will reduce the system's throughput during the communications. Since the same channel estimation should also be used by the benchmarks, we only focus our attention on the data transmission performance comparisons in this work.

[3]At least τ orthogonal pilots can be generated upon using the SVD-based method [47].

$$\mathcal{CN}\left(0,(\beta_{m,n,k}-\frac{\tau\tilde{p}_p\beta_{m,n,k}^2}{\sigma^2+\tau\tilde{p}_p\sum\limits_{n'=1}^{N}\sum\limits_{k'=1}^{K}\beta_{m,n',k'}|\boldsymbol{\varphi}_{n,k}^{\dagger}\boldsymbol{\varphi}_{n',k'}|^2})\mathbf{I}_{L_m}\right),$$

where $\beta_{m,n,k}$ denotes the large-scale fading of the link between the AP$_m$ and the DU$_{n,k}$.

Similarly, the pilot signal of the UUs received by the AP$_m$ can be expressed as

$$\mathbf{Y}_m^u=\sqrt{\tau}\tilde{p}_p\sum_{i=1}^{N_u}\mathbf{h}_{m,i}^T\boldsymbol{\varphi}_i^{\dagger}+\mathbf{N}_m, \tag{47}$$

where $\boldsymbol{\varphi}_i \in \mathbb{C}^{\tau\times 1}$ is the pilot sequence of the UU$_i$, which satisfies $\|\boldsymbol{\varphi}_i\|^2=1$, and the channel estimation error $\delta_{m,i}$ of $\mathbf{h}_{m,i}$ follows $\delta_{m,i}\sim\mathcal{CN}\left(0,(\beta_{m,i}-\frac{\tau\tilde{p}_p\beta_{m,i}^2}{\sigma^2+\tau\tilde{p}_p\sum\limits_{i'=1}^{N_u}\beta_{m,i'}|\boldsymbol{\varphi}_i^{\dagger}\boldsymbol{\varphi}_{i'}|^2})\mathbf{I}_{L_m}\right)$, where $\beta_{m,i}$ denotes the large-scale fading of the link between the AP$_m$ and the UU$_i$.

Generally, we assume that the DUs and the UUs share an orthogonal set of pilots, while the DUs in a cluster employ the same pilot signals and the users in different clusters rely on different pilots. Explicitly, for any two users k' and k in the n-th cluster, we have $\boldsymbol{\varphi}_{n,k}=\boldsymbol{\varphi}_{n,k'}$, $\boldsymbol{\varphi}_{n,k}^{\dagger}\boldsymbol{\varphi}_{n,k'}=1$, and for any two users k and $\bar{k}$ in any two clusters n and n' ($n'\neq n$), we have $\boldsymbol{\varphi}_{n',\bar{k}}^{\dagger}\boldsymbol{\varphi}_{n,k}=0$. Similarly, we have $\boldsymbol{\varphi}_i^{\dagger}\boldsymbol{\varphi}_{i'}=1$ if $i=i'$, and $\boldsymbol{\varphi}_i^{\dagger}\boldsymbol{\varphi}_{i'}=0$ otherwise.

Note that the SIC order of NOMA users is determined by the estimated channel quality, which can be expressed as

$$\pi_n(l)>\pi_n(k),\ \text{if}\ \sum_{m=1}^{M}\left|\hat{\mathbf{h}}_{m,n,l}\right|^2>\sum_{m=1}^{M}\left|\hat{\mathbf{h}}_{m,n,k}\right|^2. \tag{48}$$

It may be readily seen that the channel estimation error has a direct impact both on the beamforming and SIC order design, which may lead to a sum-rate degradation. Therefore, designing both the pilots and the channel estimation algorithm for improving the estimation accuracy as well as proposing bespoke beamforming optimization algorithms for mitigating the channel estimation error constitute our future research.

B. Comparison Benchmarks

Moreover, the following benchmarks are used for comparisons, and the frequency band occupation of each scheme is plotted in Fig. 3.

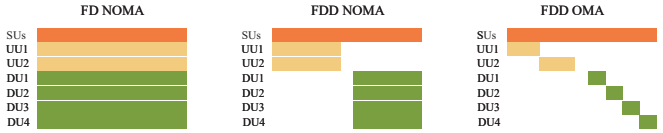

Figure 3: Illustration of frequency bands occupied by users.

- **The FD cell-based NOMA system:** A single FD-enabled AP is deployed within the specific region, whose maximal transmit power is set to $\sum_{m=1}^{M}P_{AP}^{\max}$, and its number of antennas is set to $\sum_{m=1}^{M}L_m$. NOMA is employed as the MA technique.
- **FDD cell-free NOMA system:** Multiple APs are distributed within the region for supporting the DL and UL services via the FDD technique. NOMA is employed as the MA technique.
- **FDD cell-free OMA system:** Multiple APs provide DL and UL services via FDD technique with employing OMA as the MA technique.
- **Optimized beamforming and fixed power allocation (OBFP):** The beamforming vectors of the satellite and of the APs are optimized, the PAFs of the NOMA DL set to $(0.8, 0.2)$.
- **Zero-forcing and fixed power allocation (ZF-FP):** The ZF is employed both at the satellite and at the APs, the PAFs of the NOMA DL set to $(0.8, 0.2)$, and the uplink transmit power is set to 33dBm for all UUs.

[4]The power level of residual SI varies, depending on different RF chains and antenna designs. Here, we consider the best-case conditions associated with $\rho_{SI}=-130$dB to study the maximum performance gain facilitated by the proposed system.

Table III: SIMULATION PARAMETERS [24], [43]

Parameter	Value
Noise power σ^2	-90dBm
Pilot transmit power $\tilde{p}_p$	20dBm
System bandwidth W	15MHz
Shadowed Rician channel factor (m_r, b_r, Ω_r)	(5, 0.251, 0.279)
Speed of light c	3×10^8m/s
Radius of cell-free systems	1000m
Residual SI ρ_{SI}[4]	[-110, -130]dB [24], [48]
Maximal transmit power of UUs $P_u^{\max}$	33dBm
Length of pilot sequence τ	56
Maximal transmit power of APs P_{AP}^{max}	46dBm
Carrier frequency f_c	20GHz
Maximum transmit power of satellite	60dBm
User antenna gain $\tilde{\vartheta}$	4.8dB
Satellite's 3dB beam-width $\theta_{3\text{dB}}$	0.3°
Noise Temperature T	300K
Reference distance (d_0, d_1)	$(10, 50)$m
Altitude of satellite d_h	35786km
Fixed PAFs of NOMA DL	(0.8 0.2)
Boltzman constant K_B	1.38×10^{-23}J/K
ν_s	53.45dB

C. Simulation Results

Fig. 4 portrays the system topology of the cell-free networks, where the APs, the UUs and the DUs are distributed within a 1000m radius circle, 2 SUs are served via the satellite DL, 8 APs are spread out to serve 4 DUs and 2UUs, while the DUs are assigned into 2 clusters with 2 DUs in each cluster.

Fig. 5 illustrates the convergence performance of our proposed algorithm for a random channel. The number of APs is set to 8, 4 DUs and 2UUs are simultaneously served by all APs and 2 SUs are served by the satellite DL within the same frequency band as the DUs and UUs. The number of antennas at the satellite is set to 2. As illustrated in Fig. 5, our proposed algorithm converges as the number of iterations is increase and the converged solution can be obtained in 10 iterations.

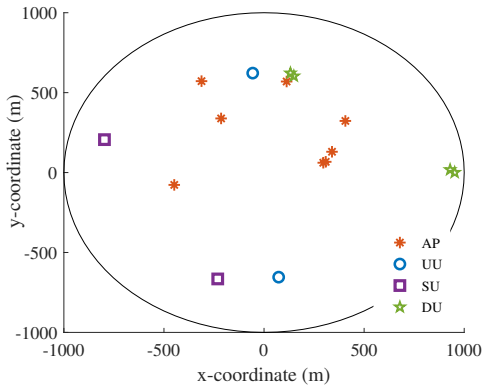

Figure 4: System topology of cell-free systems within 1000m radius circle.

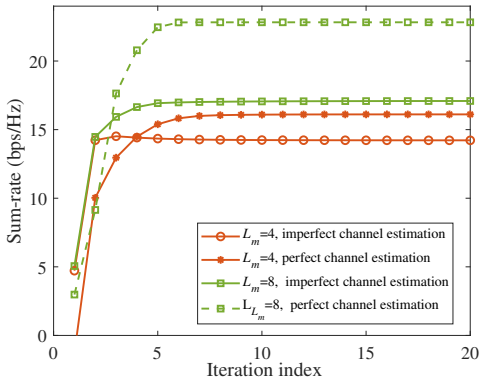

Figure 5: The convergence vs. the number of iterations.

Fig. 6 illustrates the sum-rate of our proposed FD cell-free NOMA system versus the number of APs compared to the FDD cell-free NOMA system, where both perfect and imperfect channel estimation are considered. Note that the channel estimation error is derived in Section VI-A3, and realistic imperfect SIC is considered by setting the residual SIC parameter to 0.1. The maximal transmit power of each AP is set to 46dBm, the number of antennas at each AP is set to $L_m = 4$, the number of DUs is 4, the number of satellite antennas is 2, the number of SUs is set to $N_s = 2$, the minimal required rate of the DUs, the SUs, and the UUs are set to 0.5bps/Hz, 0.5bps/Hz and 1.0bps/Hz, respectively,

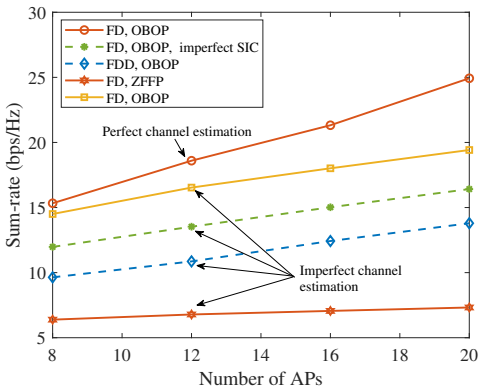

Figure 6: Sum-rate versus the number of APs.

and $\bar{\gamma} = 0.5$bps/Hz. The results indicate that 1) the sum-rate performance can be enhanced by employing the FD scheme compared to FDD systems; 2) the OBOP algorithm outperforms the conventional ZF-FP algorithm, and the performance gain of our proposed OBOP over ZF-FP becomes more pronounced as M increases; 3) the imperfect SIC will inflict additional interference, hence degrading the system performance; 4) the sum-rate increases with the number of APs, because the users are guaranteed to be near at least one AP as the density of APs increases.

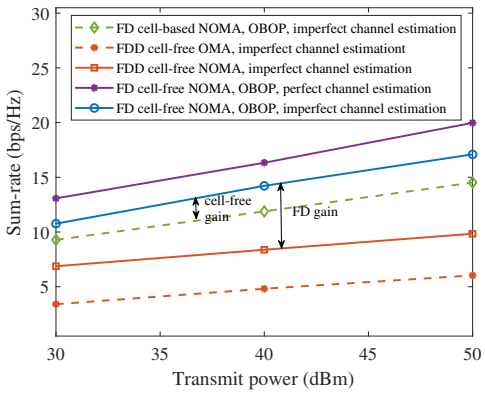

Figure 7: Sum-rate versus the maximum transmit power of each AP.

In Fig. 7, we plot the sum-rate of cell-free systems versus the maximum transmit power of the APs, where the number of APs is set to $M = 8$, the number of antennas at each AP is set to $L_m = 4$, the number of DUs is 4, the number of UUs is 2, the maximal transmit power of UUs is set to 33dBm, the residual interference parameter of imperfect SIC is set to 0.1. The performance of both the FDD and the cell-based system is also included for comparisons. It can be observed that the sum-rate increases linearly with the transmit power. However, if the transmit power is lower than 30dBm, the rate constraints may not be guaranteed due to the deleterious effects of interference and the presence of constraints, which leads to potential infeasibility. Moreover, the results also indicate that: 1) employing FD and NOMA schemes in cell-free systems is capable of significantly increasing the sum-rate by simultaneously serving the DUs and the UUs; 2) the cell-free system outperforms the cell-based system, and the performance gap between the cell-free and cell-based systems becomes more pronounced upon approaching $P_{AP}^{\max}$, which can be readily explained. Compared to the cell-based system using a single AP, the distributed APs bring the antennas closer to users, hence reducing the propagation loss. In addition, the ICI can be mitigated due to our sophisticated beamformer and transmit power allocation at each AP of the cell-free system, where some APs serve all clusters, while other only serve some clusters. By contrast, in the cell-based system, all the clusters are served by a single AP, which leads to a high ICI, despite increasing the transmit power.

Fig. 8 illustrates the sum-rate performance of the channel models in [43] and [44], where the impact of different rainfall intensities is considered [45]. The simulation parameters are

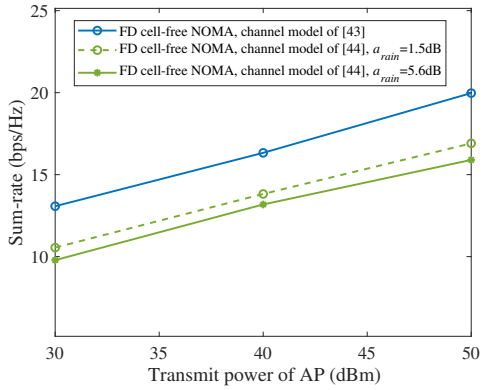

Figure 8: Sum-rate performance of different satellite channel models.

the same as in Fig. 7, and we consider perfect channel estimation. It can be observed that the sum-rate degrades upon increasing a_{rain}. This can be readily explained. Explicitly, our proposed beamforming design significantly mitigates the interference between the satellite and terrestrial networks (e.g., interference between the DUs and the SUs). However, the UUs do not have beamforming capability, hence their transmit power may be reduced upon increasing a_{rain} for mitigating their interference imposed on SUs, in order to guarantee the QoS requirements of SUs. Therefore, the UUs' rates decrease, and so does the total sum-rate. Moreover, the performance associated with the channel model of [44] shows a degradation compared to that under the channel model of [43]. This is because the channel model of [44] takes more kinds of attenuation (e.g. clutter loss) into consideration.

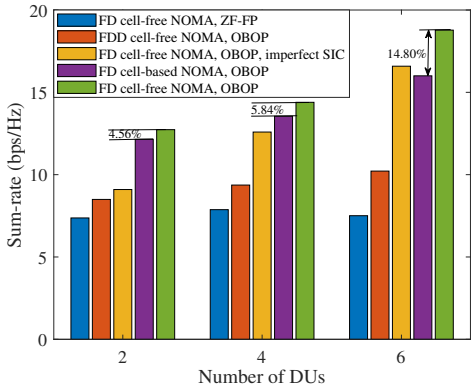

Figure 9: Sum-rate versus the number of DUs.

Fig. 9 shows the sum-rate versus the number of DUs, where the number of UUs is set to 2, all the DUs and UUs are served by 8 APs, each AP is equipped with $L_m = 4$ antennas, and has the maximal transmit power of 46dBm. The satellite is equipped with 2 antennas and it serves 2 SUs on the ground. The results indicate that: 1) the sum-rate performance increases with the number of DUs; 2) our proposed FD cell-free NOMA system outperforms the FDD and cell-based systems in terms of the sum-rate; 3) the efficiency of our proposed OBOP algorithm is validated. Furthermore, observe from Fig. 9 that the performance gain of the cell-free system over its cell-based counterpart becomes more pronounced upon increasing the number of DUs. One of the main reasons for this trend is that increasing the number of DUs increases the ICI in the cell-based system, while in the cell-free system the ICI can be mitigated by controlling the transmit power assigned to the clusters at each AP.

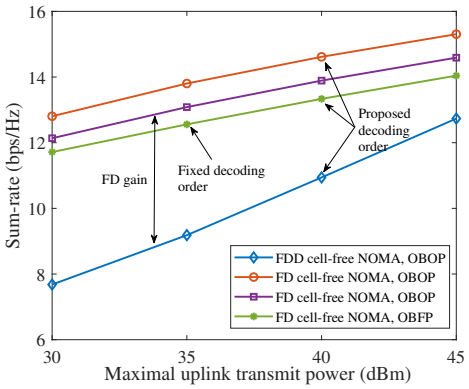

Figure 10: Sum-rate versus the maximal power of uplink users.

Fig. 10 depicts the sum-rate versus the maximal transmit power of the UUs, where 4 DUs and 2 UUs are simultaneously served by 8 APs by the FD scheme. Each AP is equipped with 4 antennas and its maximal transmit power is set to 40dBm. The number of SUs is set to $N_s = 2$, and the number of antennas at the satellite is 2. We consider both perfect and imperfect channel estimation as discussed in Section VI-A3, and also draw the performance curve of the OBFP algorithm. The results show that: 1) the FD aided cell-free system outperforms the FDD assisted system, while upon increasing the uplink transmit power, the performance gap between the FD and the FDD schemes becomes small due to the escalating CCI caused by the FD scheme; 2) our proposed OBOP algorithm achieves higher sum-rate than the OBFP, which demonstrates importance of sophisticated power allocation in the NOMA DL; 3) our proposed sophisticated SIC order design outperforms the fixed SIC order in terms of the sum-rate without any additional complexity.

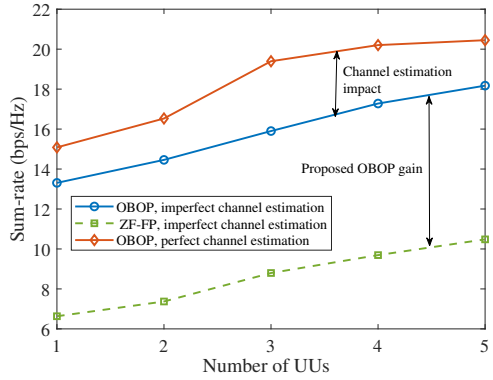

Figure 11: Sum-rate versus the number UUs.

In Fig. 11, the sum-rate versus the number of UUs is portrayed. The performance of the proposed OBOP algorithm is

compared to that of the ZF-FP algorithm, and the performance relying on realistic imperfect channel state information is also shown. The number of DUs is set to 4, served by 8 APs with the minimal required rate set to 0.5bps/Hz, and the minimal required rate of UUs is set to 1.0bps/Hz. Furthermore, 2 SUs are served by the 2-antenna satellite via the same time/frequency slot as in the cell-free system, where each SU has the minimal required rate of 0.5bps/Hz. Our simulation results indicate the sum-rate improvement attained upon increasing the number of UUs. Furthermore, the imperfect channel estimation degrades the networking performance: in both the DL and UL, because it erodes the accuracy of beamformer design and the ZF detection performance at the APs, hence degrades the power of the desired received signals as well as the interference mitigation capability.

VII. Conclusion

In this paper, a NOMA aided FD cell-free system was proposed for SGINs in order to improve the SE. The satellite serves the SUs within the same frequency band as the terrestrial cell-free systems, where the UL and DL users were simultaneously served by the FD-enabled APs within the same time- and frequency-resource. NOMA was employed as the MA technique in our cell-free systems. We formulated a sum-rate maximization problem by jointly optimizing the power allocation factors of the NOMA DL, the uplink transmit power of UUs, and the beamformer at both the satellite and APs. To solve the resultant non-convex problem, SCA and SDP methods were conceived for converting the resultant intractable problem into an equivalent convex one. Our simulation results validated that our proposed system outperforms both its conventional cell-based and FDD aided counterparts in terms of its SE, and the effectiveness of our proposed SIC order design for NOMA was validated. Moreover, future works are to study the max-min user fairness, geometric mean rate optimization [49] and bit error rate performance of our proposed system.

References

[1] Y. Yuan, S. Wang, Y. Wu, H. V. Poor, Z. Ding, X. You, and L. Hanzo, "NOMA for next-generation massive IoT: Performance potential and technology directions," *IEEE Commun. Mag.*, vol. 59, no. 7, pp. 115–121, 2021.

[2] H. Zhang, C. Jiang, J. Wang, L. Wang, Y. Ren, and L. Hanzo, "Multicast beamforming optimization in cloud-based heterogeneous terrestrial and satellite networks," *IEEE Trans. Veh. Technol.*, vol. 69, no. 2, pp. 1766–1776, 2020.

[3] Q. Huang, M. Lin, W.-P. Zhu, J. Cheng, and M.-S. Alouini, "Uplink massive access in mixed RF/FSO satellite-aerial-terrestrial networks," *IEEE Trans. Commun.*, vol. 69, no. 4, pp. 2413–2426, 2021.

[4] P. Botsinis, D. Alanis, C. Xu, Z. Babar, D. Chandra, S. X. Ng, and L. Hanzo, "Air-to-ground NOMA systems for the "Internet-above-the-clouds"," *IEEE Access*, vol. 6, pp. 47 442–47 460, 2018.

[5] J. Yang, D. Li, X. Jiang, S. Chen, and L. Hanzo, "Enhancing the resilience of low earth orbit remote sensing satellite networks," *IEEE Netw.*, vol. 34, no. 4, pp. 304–311, 2020.

[6] Z. Yin, N. Cheng, T. H. Luan, Y. Hui, and W. Wang, "Green interference based symbiotic security in integrated satellite-terrestrial communications," *IEEE Trans. Wireless Commun.*, Early Access, 2022, doi: 10.1109/TWC.2022.3181277.

[7] P. K. Sharma, P. K. Upadhyay, D. B. da Costa, P. S. Bithas, and A. G. Kanatas, "Performance analysis of overlay spectrum sharing in hybrid satellite-terrestrial systems with secondary network selection," *IEEE Trans. Wireless Commun.*, vol. 16, no. 10, pp. 6586–6601, 2017.

[8] Z. Gao, Z. Wan, D. Zheng, S. Tan, C. Masouros, D. W. K. Ng, and S. Chen, "Integrated sensing and communication with mmwave massive MIMO: A compressed sampling perspective," *IEEE Transactions on Wireless Communications*, pp. 1–1, 2022.

[9] Y. Zhang, L. Yin, C. Jiang, and Y. Qian, "Joint beamforming design and resource allocation for terrestrial-satellite cooperation system," *IEEE Trans. Commun.*, vol. 68, no. 2, pp. 778–791, 2019.

[10] B. Deng, C. Jiang, J. Yan, N. Ge, S. Guo, and S. Zhao, "Joint multigroup precoding and resource allocation in integrated terrestrial-satellite networks," *IEEE Trans. Veh. Technol.*, vol. 68, no. 8, pp. 8075–8090, 2019.

[11] D. Peng, A. Bandi, Y. Li, S. Chatzinotas, and B. Ottersten, "Hybrid beamforming, user scheduling, and resource allocation for integrated terrestrial-satellite communication," *IEEE Trans. Veh. Technol.*, vol. 70, no. 9, pp. 8868–8882, 2021.

[12] S. Kusaladharma, W.-P. Zhu, W. Ajib, and G. A. A. Baduge, "Achievable rate characterization of NOMA-aided cell-free massive MIMO with imperfect successive interference cancellation," *IEEE Trans. Commun.*, vol. 69, no. 5, pp. 3054–3066, 2021.

[13] M. Bashar, K. Cumanan, A. G. Burr, H. Q. Ngo, L. Hanzo, and P. Xiao, "On the performance of cell-free massive MIMO relying on adaptive NOMA/OMA mode-switching," *IEEE Trans. Commun.*, vol. 68, no. 2, pp. 792–810, 2020.

[14] Y. Zhang, M. Zhou, X. Qiao, H. Cao, and L. Yang, "On the performance of cell-free massive MIMO with low-resolution ADCs," *IEEE Access*, vol. 7, pp. 117 968–117 977, 2019.

[15] J. Zhang, S. Chen, Y. Lin, J. Zheng, B. Ai, and L. Hanzo, "Cell-free massive MIMO: A new next-generation paradigm," *IEEE Access*, vol. 7, pp. 99 878–99 888, 2019.

[16] E. Sharma, R. Budhiraja, K. Vasudevan, and L. Hanzo, "Full-duplex massive MIMO multi-pair two-way AF relaying: Energy efficiency optimization," *IEEE Trans. Commun.*, vol. 66, no. 8, pp. 3322–3340, 2018.

[17] M. Vaezi, G. A. A. Baduge, Y. Liu, A. Arafa, F. Fang, and Z. Ding, "Interplay between NOMA and other emerging technologies: A survey," *IEEE Trans. on Cogn. Commun. Netw.*, vol. 5, no. 4, pp. 900–919, 2019.

[18] L. Dai, B. Wang, Z. Ding, Z. Wang, S. Chen, and L. Hanzo, "A survey of non-orthogonal multiple access for 5G," *IEEE Communications Surveys & Tutorials*, vol. 20, no. 3, pp. 2294–2323, 2018.

[19] X. Zhu, C. Jiang, L. Kuang, N. Ge, and J. Lu, "Non-orthogonal multiple access based integrated terrestrial-satellite networks," *IEEE J. Sel. Areas Commun.*, vol. 35, no. 10, pp. 2253–2267, 2017.

[20] X. Liu, K.-Y. Lam, F. Li, J. Zhao, L. Wang, and T. S. Durrani, "Spectrum sharing for 6G integrated satellite-terrestrial communication networks based on NOMA and CR," *IEEE Netw.*, vol. 35, no. 4, pp. 28–34, 2021.

[21] F. Rezaei, C. Tellambura, A. A. Tadaion, and A. R. Heidarpour, "Rate analysis of cell-free massive MIMO-NOMA with three linear precoders," *IEEE Trans. Commun.*, vol. 68, no. 6, pp. 3480–3494, 2020.

[22] T. K. Nguyen, H. H. Nguyen, and H. D. Tuan, "Max-min QoS power control in generalized cell-free massive MIMO-NOMA with optimal backhaul combining," *IEEE Trans. Veh. Technol.*, vol. 69, no. 10, pp. 10 949–10 964, 2020.

[23] Q. N. Le, V.-D. Nguyen, O. A. Dobre, N.-P. Nguyen, R. Zhao, and S. Chatzinotas, "Learning-assisted user clustering in cell-free massive MIMO-NOMA networks," *IEEE Trans. Veh. Technol.*, vol. 70, no. 12, pp. 12 872–12 887, 2021.

[24] H. V. Nguyen, V.-D. Nguyen, O. A. Dobre, S. K. Sharma, S. Chatzinotas, B. Ottersten, and O.-S. Shin, "On the spectral and energy efficiencies of full-duplex cell-free massive MIMO," *IEEE J. Sel. Areas Commun.*, vol. 38, no. 8, pp. 1698–1718, 2020.

[25] Z. Lin, M. Lin, J.-B. Wang, T. de Cola, and J. Wang, "Joint beamforming and power allocation for satellite-terrestrial integrated networks with non-orthogonal multiple access," *IEEE J. Sel. Topics Signal Process.*, vol. 13, no. 3, pp. 657–670, 2019.

[26] S. Kusaladharma, W. P. Zhu, W. Ajib, and G. A. A. Baduge, "Stochastic geometry based performance characterization of SWIPT in cell-free massive MIMO," *IEEE Trans. Veh. Technol.*, vol. 69, no. 11, pp. 13 357–13 370, 2020.

[27] E. Nayebi, A. Ashikhmin, T. L. Marzetta, H. Yang, and B. D. Rao, "Precoding and power optimization in cell-free massive MIMO systems," *IEEE Trans. Wireless Commun.*, vol. 16, no. 7, pp. 4445–4459, 2017.

[28] P. Wang, J. Zhang, X. Zhang, Z. Yan, B. G. Evans, and W. Wang, "Convergence of satellite and terrestrial networks: A comprehensive survey," *IEEE Access*, vol. 8, pp. 5550–5588, 2019.

[29] T. Taleb, Y. Hadjadj-Aoul, and T. Ahmed, "Challenges, opportunities, and solutions for converged satellite and terrestrial networks," *IEEE Wireless Commun.*, vol. 18, no. 1, pp. 46–52, 2011.

[30] K. An, M. Lin, W.-P. Zhu, Y. Huang, and G. Zheng, "Outage performance of cognitive hybrid satellite–terrestrial networks with interference constraint," *IEEE Trans. Veh. Technol.*, vol. 65, no. 11, pp. 9397–9404, 2016.

[31] C. Zhang, C. Jiang, L. Kuang, J. Jin, Y. He, and Z. Han, "Spatial spectrum sharing for satellite and terrestrial communication networks," *IEEE Trans. Aerosp. Electron. Syst.*, vol. 55, no. 3, pp. 1075–1089, 2019.

[32] Y.-C. Liang, J. Tan, H. Jia, J. Zhang, and L. Zhao, "Realizing intelligent spectrum management for integrated satellite and terrestrial networks," *Journal of Communications and Information Networks*, vol. 6, no. 1, pp. 32–43, 2021.

[33] L. Wang, Y. Wu, H. Zhang, S. Choi, and V. C. Leung, "Resource allocation for NOMA based space-terrestrial satellite networks," *IEEE Trans. Wireless Commun.*, vol. 20, no. 2, pp. 1065–1075, 2020.

[34] H. Li, S. Zhao, Y. Li, and C. Peng, "Sum secrecy rate maximization in NOMA-based cognitive satellite-terrestrial network," *IEEE Wireless Commun. Lett.*, vol. 10, no. 10, pp. 2230–2234, 2021.

[35] X. Tang, K. An, K. Guo, Y. Huang *et al.*, "Outage analysis of non-orthogonal multiple access-based integrated satellite-terrestrial relay networks with hardware impairments," *IEEE Access*, vol. 7, pp. 141 258–141 267, 2019.

[36] L. Han, W.-P. Zhu, and M. Lin, "Outage analysis of NOMA-based multiple-antenna hybrid satellite-terrestrial relay networks," *IEEE Commun. Lett.*, vol. 25, no. 4, pp. 1109–1113, 2021.

[37] M. Farooq, H. Q. Ngo, E.-K. Hong, and L.-N. Tran, "Utility maximization for large-scale cell-free massive MIMO downlink," *IEEE Trans. Commun.*, vol. 69, no. 10, pp. 7050–7062, 2021.

[38] H. Yu, N. Ye, and A. Wang, "Non-orthogonal wireless backhaul design for cell-free massive MIMO: An integrated computation and communication approach," *IEEE Wireless Commun. Lett.*, vol. 10, no. 2, pp. 281–285, 2021.

[39] H. Q. Ngo, A. Ashikhmin, H. Yang, E. G. Larsson, and T. L. Marzetta, "Cell-free massive MIMO versus small cells," *IEEE Trans. Wireless Commun.*, vol. 16, no. 3, pp. 1834–1850, 2017.

[40] B. Wang, J. Wang, J. Fang, H. Duan, and H. Li, "Efficient max-min power control for cell-free massive MIMO systems: An alternating projection-based approach," *IEEE Signal Process. Lett.*, vol. 28, pp. 2102–2106, 2021.

[41] Y. Li and G. A. Aruma Baduge, "NOMA-aided cell-free massive MIMO systems," *IEEE Wireless Commun. Lett.*, vol. 7, no. 6, pp. 950–953, 2018.

[42] X. Sun, N. Yang, S. Yan, Z. Ding, D. W. K. Ng, C. Shen, and Z. Zhong, "Joint beamforming and power allocation in downlink NOMA multiuser MIMO networks," *IEEE Trans. Wireless Commun.*, vol. 17, no. 8, pp. 5367–5381, 2018.

[43] P. K. Sharma, D. Deepthi, and D. I. Kim, "Outage probability of 3-D mobile UAV relaying for hybrid satellite-terrestrial networks," *IEEE Commun. Lett.*, vol. 24, no. 2, pp. 418–422, 2020.

[44] 3GPP, "Study no New Radio (NR) to support nonterrestrial networks (Release 15)," 3rd Generation Partnership Project (3GPP), Technical Specification (TS) 38.811, version 15.

[45] X. Liang, J. Jiao, B. Feng, S. Wu, B. Cao, and Q. Zhang, "Performance analysis of millimeter-wave hybrid satellite-terrestrial relay networks over rain fading channel," in *2018 IEEE 88th Vehicular Technology Conference (VTC-Fall)*, 2018, pp. 1–5.

[46] M. Duarte, C. Dick, and A. Sabharwal, "Experiment-driven characterization of full-duplex wireless systems," *IEEE Trans. Wireless Commun.*, vol. 11, no. 12, pp. 4296–4307, 2012.

[47] O. Edfors, M. Sandell, J.-J. van de Beek, S. Wilson, and P. Borjesson, "OFDM channel estimation by singular value decomposition," *IEEE Trans. Commun.*, vol. 46, no. 7, pp. 931–939, 1998.

[48] M. Elsayed, A. A. A. El-Banna, O. A. Dobre, W. Shiu, and P. Wang, "Hybrid-layers neural network architectures for modeling the self-interference in full-duplex systems," *IEEE Trans. Veh. Technol.*, vol. 71, no. 6, pp. 6291–6307, 2022.

[49] H. Yu, H. D. Tuan, E. Dutkiewicz, H. V. Poor, and L. Hanzo, "Maximizing the geometric mean of user-rates to improve rate-fairness: Proper vs. improper gaussian signaling," *IEEE Trans. Wireless Commun.*, vol. 21, no. 1, pp. 295–309, 2022.

BIOGRAPHY SECTION

Qiling Gao received the B.Eng. degree in Information and Communication Engineering from Harbin Engineering University, Harbin, China, in 2018. She is currently working toward her Ph.D. at the School of Electronics and Information Engineering, Harbin Institute of Technology. Her research interests include non-orthogonal multiple access and resource allocation.

Min Jia (Senior Member, IEEE) received the M.Sc. degree in Information and Communication Engineering from Harbin Institute of Technology (HIT) in 2006, and the Ph.D. degree from the SungKyungKwan University and HIT in 2010. She is currently a Professor and the Ph.D. supervisor at the School of Electronics and Information Engineering in HIT. Her research interests focus on advanced mobile communication technology for LTE and 5G, cognitive radios, digital signal processing, and advanced broadband satellite communication systems.

She has won six best paper awards at several international conferences. She is the General Chair of the IEEE GLOBECOM 2019 Workshop Intelligent and Cognitive Space, Terrestrial and Ocean Internet, Systems and Applications. She is also a member of the Steering Committee of the WiSATs international conference. She is also the winner of Science Fund for Excellent Young Scholars for Heilongjiang Province

Qing Guo (Member, IEEE) received a B.S. degree in radio engineering from the Beijing Institute of Posts and Telecommunications in 1985 and the M.S. and Ph.D. degrees in information and communication engineering from the Harbin Institute of Technology, Harbin, China, in 1990 and 1998, respectively. He is currently a Professor at the School of Electronics and Information Engineering, Harbin Institute of Technology, and the Director of the Key Laboratory of Wideband Wireless Communications and Networks, Heilongjiang.

Xuemai Gu (Member, IEEE) received the M.Sc. and Ph.D. degrees from the Department of Information and Communication Engineering, Harbin Institute of Technology, in 1985 and 1991, respectively. He is currently a Professor and the President of the Graduate School, HIT. His research interests focus on integrated and hybrid satellite and terrestrial communications and broadband multimedia communication techniques.

Lajos Hanzo (FIEEE'04) (http://www-mobile.ecs.soton.ac.uk, https://en.wikipedia.org/wiki/Lajos_Hanzo) received Honorary Doctorates from the Technical University of Budapest and Edinburgh University. He is a Foreign Member of the Hungarian Science-Academy, Fellow of the Royal Academy of Engineering (FREng), of the IET, of EURASIP and holds the IEEE Eric Sumner Technical Field Award.